Antimicrobials and Antimicrobial Resistance

Mres.

Dimitra Panagiotopoulou

Supervisors: Dr. Manuel Banzhaf (University of Birmingham) and Dr. Stephan Heeb (University of Nottingham)

Submitted: 31/07/2020

Word count: 22741

Abstract

The discovery of penicillin has revolutionised the field of modern medicine. However, misuse and overconsumption of antibiotics have led to the rise of antimicrobial resistance (AMR). The prevalence of AMR and the lack of novel antimicrobial therapies threaten to bring society back to the pre-antibiotic era. Therefore, it is imperative to develop state-of-the-art antimicrobial strategies which can be achieved by expanding our understanding of the biology of pathogenic bacteria. This report details three AMR research projects with the first focussing on the control of the three *Escherichia coli* peptidoglycan amidases by two new regulatory proteins, YraP and NlpI. Direct interactions between YraP and amidases were investigated by employing pull-down assays however the results were inconclusive. Also, the effect of NlpI on the hydrolytic activity of amidases *in vitro* was explored, detecting no change in the activity of AmiA amidase. The second project examined the methodology of Next Generation Sequencing (NGS) data analysis. For this purpose, publicly available raw sequence data from a publication on *Pseudomonas aeruginosa* global clone ST395 were used. Overall, the computational pipeline used here produced different results to that of the publication which shows the dependence of the outcome on the choice of bioinformatic programmes. In the last chapter, a new small non-coding RNA, the PqsX, is studied along with its potential roles in the regulation of the *pqs* Quorum Sensing (QS) system of *P. aeruginosa*. The *pqs* system controls the expression of virulence factors which makes it a significant target for the development of antivirulent therapies.

Acknowledgements

I would like to thank Dr. Banzhaf for his guidance and teaching during my first rotation at the University of Birmingham. Thanks should also be given to Dr. Moynihan and Dr. Bryant for their advice and help with the experimental procedures. Special gratitude must be given to Dr. Heeb and Professor Cámara for their guidance and valuable advice over the second rotation, at the University of Nottingham. I am thankful to Natalia Romo Catalan for the aid and supervision in the lab. I would also like to thank Professor Williams, Dr. Hardie, and Professor van Schaik for their support throughout the programme. I am greatly thankful to the Wellcome Trust for funding this research programme.

Table of Contents

List of Figures

List of Tables

Abbreviations

AMR	Antimicrobial Resistance
AQ	2-alkyl-4(1*H*)-quinolone
ARG	Antimicrobial Resistance Gene
CDC	Centers for Disease Control and Prevention
CF	Cystic Fibrosis
EMSA	Electrophoretic Mobility Shift Assay
GARDP	Global Antibiotic Research and Development Partnership
GI	Genomic Island
GLASS	Global Antimicrobial Resistance Surveillance System
HHQ	2-heptyl-4-hydroxyquinoline (HHQ)
IACG	UN Interagency Coordinating Group on Antimicrobial resistance
IM	Inner Membrane
MDR	Multidrug Resistant
MLST	Multi Locus Sequence Type
NGS	Next Generation Sequencing
OM	Outer Membrane
PG	Peptidoglycan
PQS	Pseudomonas Quinolone Signal, 2-heptyl-3-hydroxy-4-quinolone
PYO	Pyocyanin
QS	Quorum Sensing
R&D	Research and Development
RBS	Ribosome Binding Site
SNP	Single Nucleotide Polymorphism
sRNA	Small non-coding RNA
ST	Sequence Type
TSS	Transcription Start Site
UTR	Untranslated Transcribed Region
WHO	World Health Organisation
CCDEP	Centre for Disease Dynamics Economics & Policy
MST	MicroScale Thermophoresis

HQNO 2-heptyl-4-hydroxyquinoline *N*-oxide

Chapter 1: Introduction

More than 100 years have elapsed since Paul Ehrlich envisioned *Zauberkugel*, the magic bullet. It is the concept that, like a bullet, a dye-like compound can specifically target and kill causal agents of a disease leaving host cells unharmed[1]. This vision has been materialised since then by the discovery and use of chemical compounds, called antimicrobials, which can kill or inhibit the growth of microorganisms. However, microbes may possess or develop mechanisms against antimicrobials making them less susceptible to antibiotics, a phenomenon called antimicrobial resistance (AMR). Currently, antimicrobials find uses in various aspects of modern medicine, in addition to prophylaxis and boosting animal growth livestock [2,3]. All these activities could soon belong to the past due to the ever-increasing AMR in pathogenic microorganisms.

Globally, 700,000 people die from AMR infections annually. According to the UN Interagency Coordinating Group on Antimicrobial resistance (IACG), AMR could be responsible for up to 10 million deaths each year surpassing cancer mortalities, and for the impoverishment of 24 million people by 2050 [4]. The threat is emphasised by prevalence of the multidrug-resistant (MDR) 'ESKAPE' organisms (*Enterococcus* spp., *Staphylococcus aureus*, *Klebsiella* spp., *Acinetobacter baumannii*, *P. aeruginosa,* and *Enterobacter* spp.) that are responsible for a number of formidable nosocomial infections. The need for new worldwide policies and extensive research is therefore palpable.

History of Antibiotics

Contrary to popular belief, penicillin was not the first natural antibiotic ever discovered. In 1896, an Italian physician named Bartolomeo Gosio isolated in crystal form mycophenolic acid (MPA, or mycophenolate), a product of *Penicillium brevicompactum* [5]. This substance inhibited *Bacillus anthracis* growth and was proven later that it also possessed antiviral, antifungal, antitumor, and anti-psoriasis properties [5]. Unfortunately, the publication of the findings was in Italian and so it went under the radar until its rediscovery by the Americans in 1913 [5]. In 1909, Paul Ehrlich and his assistant discovered compound 606, also known as Salvarsan, which rapidly became the standard treatment for syphilis.

Despite the early introduction of chemical compounds for infection treatment, the field of chemotherapy was revolutionised only after the discovery of penicillin. After returning from his holidays in September 1928, the bacteriologist Alexander Fleming observed that one of his *S. aureus* plates had been contaminated by a mould and the zone immediately around it was clear of bacterial colonies [6]. He deducted that the fungus excreted a bacterial growth inhibitory molecule. He named it penicillin after the producing fungal species *Penicillium chrysogenum*. With the collaboration of three researchers from Oxford University (Walter Florey, Ernst Boris Chain and Norman Heatley), penicillin was eventually isolated and became publicly available in 1945, saving millions of lives and heralding the advent of antibiotic era [5].

Since then, the field of natural antibiotics had been expanded exponentially to include cephalosporins, sulphonamides, and aminoglycosides, among many others. Streptomycin, a member of the aminoglycoside group, proved an important milestone thanks to its potency against *Mycobacterium tuberculosis* [5,7]. The 1950s and 1960s, characterised as the golden era of antibiotics, experienced a bloom in synthetic antibacterial compounds such as trimethoprim (as reviewed in [8]), followed by a sudden drop in discovery of new antibiotic classes. The approach to fill the void of new antimicrobials has been the modification of those already existing, albeit a short-sighted solution since resistance easily develops.

In parallel, resistance to a newly discovered antibiotic emerged from the microbial population. The first bacterial species identified resistant to penicillin was in 1940, five years before the famous antibiotic reached the public [9]. The increasing rate of penicillin resistance demanded a new solution and in 1959 methicillin was introduced in medical treatments. Less than a year later, the first methicillin-resistant *S. aureus* strains (MRSA) [10]. The oldest MRSA strain is traced back 14 years before the therapeutic use of methicillin [11]. This exemplifies that AMR is naturally present in the microbial population, but it is selected for under increased antibiotic concentrations in the environment. Additionally, vancomycin resistance was firstly documented less than six years after broad clinical use of vancomycin in 1980 [12,13]. Similar patterns arose for ceftazidime and daptomycin resistance [14,15].

Mode of action of Antibiotics

Natural antibiotics are secondary metabolites of low molecular weight and the majority of them in medical use have been isolated from soil *Actinomycetes*. Even though one of the established roles of antibiotics is as a weapon in antagonistic microbial relationships, antibiotics in natural habitats do not always reach lethal concentrations[16]. It is hypothesised that antibiotics might represent signalling molecules [17]. In subinhibitory concentrations, they can cause profound changes in the microbial populations, both on the producers and the neighbouring species. These changes include rise in protein excretion, differential effects on biofilm formation, regulation of specialized metabolic pathways, promoting evolution by increasing mutagenesis rates and horizontal gene transfer, as well as positively affecting growth [16,18].

In general, the majority of antibiotics target four essential cellular functions: DNA synthesis and translation; cell envelope and folic acid metabolism (fig. 1). Antibiotics are classified into two categories depending on their mode of action: bactericidal, if they kill the bacterium or bacteriostatic, if they arrest growth without killing the cells [19]. Antibiotics can have broad or narrow spectrum of activity, and they exhibit diverse chemical structures and properties. [20]. Major antibiotic classed employed in antibacterial therapies are listed in table 1.

Mechanisms of AMR

Antibiotic resistance genes (ARGs) occur naturally in microbial populations. An in-depth metagenomic analysis of a 30,000-year-old permafrost sediment identified various genes encoding for resistance to β-lactam, tetracycline, and glycopeptide antibiotics [38]. However, only in the past 100 years have they witnessed massive prevalence in hospitals, communities, and the environment concomitant with the extensive use of antibiotics [39,40].

AMR can either be intrinsic or acquired. Intrinsic resistance is normally chromosome-encoded and includes non-specific efflux pumps, penetration barriers, and drug-inactivating enzymes [41]. Conversely, acquired resistance is encoded on mobile genetic elements and consists of drug-specific efflux pumps, target- and drug- modifying enzymes [41]. Resistance mechanisms fall into four

major categories: drug inactivation, target modification, bypassing mechanisms, and reduced drug accumulation (fig. 2).

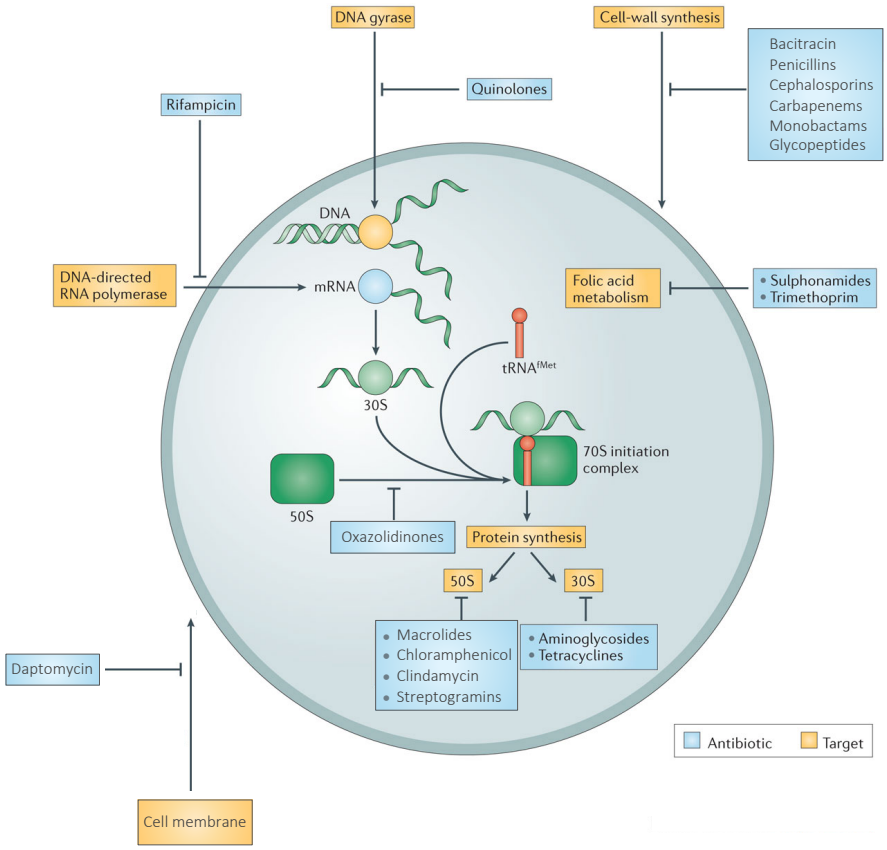

Figure 1. Mechanisms of action of antibiotics. Four main metabolic pathways are disrupted by the majority of antibiotics: translation, DNA synthesis, folate biosynthesis and cell wall metabolism. Macrolides, lincosamides (clindamycin), and streptogramin B dissociate the peptidyl-tRNA from the ribosome[21]. Phenicols (chloramphenicol) and streptogramin A disrupt the peptidyl-transferase activity of the 50S ribosomal subunit [22,23], while aminoglycosides and tetracyclines hinder tRNA entrance to the A-site [24,25]. Translation initiation is perturbed by oxazolidinones [26,27]. Quinolones stabilise DNA-topoisomerase complexes whereby introducing DNA breakages [28]. Rifamycins, represented here by rifampicin, suppresses RNA synthesis polymerase [20,29]. Glycopeptides, bacitracin (a polypeptide), and β-lactams (penicillins, cephalosporins, carbapenems, monobactams) block cell wall synthesis [30–32]. Sulphonamides and pyrymidines (trimethoprim) target enzymes of the folic acid metabolism [33,34]. The lipopeptide daptomycin depolarises cell membrane [28]. Adapted from [35]

Antibiotic class	Example	Target	Bacteriostatic or Bactericidal	Mechanism of resistance
β-lactams	Penicillins	Peptidoglycan biosynthesis	Bactericidal	Hydrolysis Efflux Altered target
Aminoglycosides	Gentamycin	Translation	both	Phosphorylation Acetylation Nucleotidylation Efflux Altered target
Glycopeptides	Vancomycin	Peptidoglycan biosynthesis	Both	Metabolic bypass
Tetracyclines	Minocycline	Translation	Bacteriostatic	Monooxygenation Efflux Altered target
Macrolides	Erythromycin	Translation	Bacteriostatic	Hydrolysis Glycosyliosis Phosphorylation Efflux Altered target
Lincosamides	Clindamycin	Translation	Bacteriostatic	Nucleotidylation Efflux Altered target
Streptogramins	Streptogramin A Streptogramin B	Translation	Bacteriostatic (bactericidal in combination)	C-O lyase (type B streptogramins) Acetylation (type A streptogramins) Efflux Altered target
Oxazolidinones	Linezolid	Translation	Bactericidal	Efflux Altered target
Phenicols	Chloramphenicol	Translation	Both	Acetylation Efflux Altered target
Quinolones	Ciprofoxacin	DNA replication	Bactericidal	Acetylation Efflux Altered target
Pyrimidines	Trimethoprim	Folate synthesis	Bacteriostatic	Efflux Altered target
Sulphonamides	Sulphamethoxazole	Folate synthesis	Bacteriostatic	Efflux Altered target
Rifamycins	Rifampicin	Transcription	Both	ADP-ribosylation Efflux Altered target
Lipopeptides	Daptomycin	Cell membrane	Bactericidal	Altered target
Polypeptides	Bacitracin	Cell membrane	Bactericidal	Efflux Altered target

Table 1. Antibiotic classes and mechanisms of microbial resistance. Adapted from [36]. The bactericidal/bacteriostatic effect depends on the species tested and antibiotic concentration [19,37]

Drug inactivation

Many bacteria encode enzymes that act upon toxic molecules, irreversibly modifying and inactivating them. Such enzymes are β-lactamases and chloramphenicol acetyltransferases [42]. An extensively studied enzyme is β-lactamase that binds to β-lactam antibiotics and hydrolyses their β-lactam ring, thus inactivating them. Extended-spectrum β-lactamase (ESBL) producing *Enterobacteriaceae* are a major concern as they are common causes of urinary tract infections [43].

Target modification

Another way of circumventing antibiotic effects is modifying the target of an antibiotic via spontaneous genetic mutations, post-translational addition of chemical groups, or reduction of the available targets [44]. Examples are mutations in the gyrase gene *gyrA* which is targeted by fluoroquinolones; and methylation of 23S rRNA conferring resistance to macrolides, lincosamides, and streptogramin[44].

Bypass pathways

An unconventional approach of some Gram-positive bacteria against vancomycin is employing alternative biosynthetic pathways for constructing their cell wall which are insensitive to vancomycin [44]. Another example is the expression of an alternative fatty acid synthase for resistance to platensimycin by *Streptomyces platensis* [45].

Restricted antibiotic accumulation

Usually, intracellular antibiotic concentration requires a minimum threshold for the antibiotic to become effective. Microbes employ three main mechanisms to reduce antibiotic accumulation. Firstly, they encode broad- or narrow-range efflux pumps that eject toxic molecules, for example the AcrAB-TolC complex of *E. coli*, which pumps out a variety of drugs [46]. Secondly, the outer membrane of Gram-negative bacteria acts as a natural barrier to antibiotic penetration (OM). Lastly, deactivation of OM porins can confer AMR by restricting entrance to hydrophilic antibiotics, as is the case of OprD porin of *P. aeruginosa* [47].

Genetic modifications

Pathogens often become intrinsically resistant to antibiotics due to genetic mutations. Genetically encoded AMR can be attained via point mutations in the coding sequence and promoter region of the antibiotic target, or gene duplication resulting in overexpression [41]. Apart from establishing mutations in genes that confer AMR, bacteria enrich their genome via horizontal gene transfer (HGT). In this case, commensal, environmental and pathogenic bacteria together form a reservoir of antibiotic resistance genes called the resistome, which can be disseminated among pathogens. Out of the three HGT mechanisms (conjugation, transformation and transduction), conjugation bears a key role in spread of ARGs[48]. ARGs are commonly associated with mobile genetic elements, such as plasmids and transposons, which facilitate transport in and between species [48].

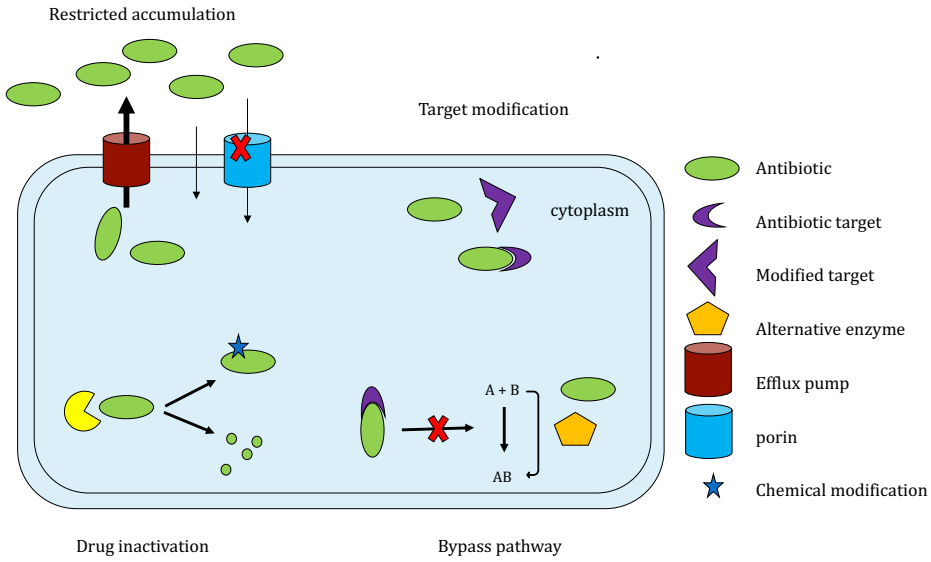

Figure 2. Mechanisms of AMR. There are four main mechanisms of AMR: reduced intracellular drug accumulation, which is facilitated by expressing efflux pumps, deactivating porins through which drugs enter the cell, and the existence of cell envelope; modifying the antibiotic target rendering it inaccessible to the antibiotic; antibiotic destruction or deactivation and ;expressing an alternative metabolic pathway which bypasses the one affected by the antibiotic.

Global dissemination of AMR

The landscape of AMR isolates is diverse around the globe. The proportion of resistant bacteria to antibiotics varies tremendously. The project ResistanceMaps of the Center for Disease Dynamics Economics & Policy (CCDEP) contains

interactive maps which show the worldwide presence of pathogens depending on their resistance to various antibiotics. By examining these maps, the heterogeneity of AMR distribution can be seen. For example, in the case of *Enterococcus faecium,* aminopenicillin isolates are prevalent in all countries for which data are included, whereas vancomycin-resistant strains are mostly found in the USA and South America (The Center for Disease Dynamics, Economics & Policy. ResistanceMap 2020). Having a closer look at Europe, a repeating pattern emerges. Overall, Mediterranean and eastern countries exhibit higher AMR levels than western and northern regions, as reported by European Centre for Disease Prevention and Control (ECDC) surveillance data for the year 2018 [50] (fig. 3).

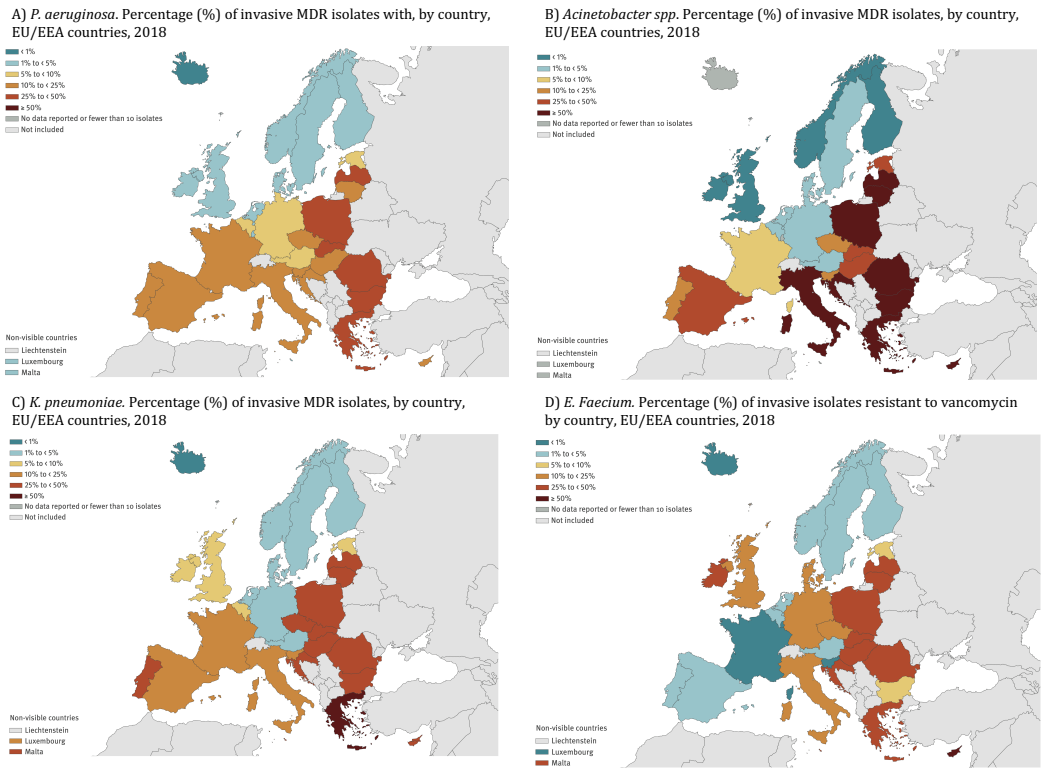

Figure 3. Dissemination of four AMR strains in EU/EEA countries in 2018, according to the ECDC report. Specifically, in Italy and Greece, the proportion of MDR *Acinetobacter spp.* is over 50%, at least 50 times higher than in the United Kingdom and Scandinavia. Likewise, *MDR P. aeruginosa* and *K. pneumoniae* are more frequent in the Mediterranean than more northerly regions. *However*, *vancomycin-resistant E. faecium* does not follow the above trend. A) *P. aeruginosa* with combined resistance (resistance to three or more antimicrobial groups among piperacillin ± tazobactam, ceftazidime, fluoroquinolones, aminoglycosides and carbapenems. B) *Acinetobacter spp*. resistant to fluoroquinolones, aminoglycosides and carbapenems. C) *K. pneumoniae*, resistant to fluoroquinolones, third-generation cephalosporins and aminoglycosides, D) *E. faecium* resistant to vancomycin.

Causes of AMR

A series of factors have played their role in the rise of AMR. The main causes are possibly the misuse and overuse of antibiotics in both medical and agricultural sectors. It has been estimated that in some states in the USA, the average number of antibiotic treatments prescribed per year exceeds the population size [51]. Moreover, in certain countries antibiotic distribution is poorly regulated and people can purchase them over the counter or online [52]. Another driving force is the incorrect antibiotic prescription. A study by Fleming-Dutra *et al*. (2016) assessed that up to half of the total outpatient antibiotic prescription in the USA were unnecessary [53].

In the agricultural sector, antibiotics have been utilised in subinhibitory concentrations as growth agents and for disease prevention in livestock for many decades. Approximately 80% of antibiotics sold in the USA are meant for the food industry with the vast majority of them ending up in the environment through animal excretion [54].

Another contributing factor may be poor hygiene, for example inadequate hand washing and improper cleaning of contaminated surfaces. Such practices could facilitate spread of AMR pathogens, especially in hospital settings [55,56]. In addition, international travel enables rapid transmission of ARGs and AMR pathogens across continents [57,58]. Taken together, these factors could create an evolutionary selective pressure for the spread and acquisition of AMR due to exposure of pathogens to low antibiotic concentrations and wide distribution.

A current disadvantage of antibiotic development is the immense cost and time for manufacturing. On average, R&D of anti-infective drugs could take around 15-20 years, and could cost more than $1.5 billion [59] with only 5% success rate [60]. Furthermore, antibiotics are used for short periods of time and emergence of resistance could render them obsolete relatively quickly [54]. Large pharmaceutical companies have abandoned antimicrobial development putting a pressure on smaller companies which are often driven to bankruptcy, as was the case of Achaogen [61,62]. Consequently, investment on antimicrobials has declined because they are perceived as less profitable and riskier than drugs for chronic conditions

such as diabetes and cancer [63,64]. As a result, fewer antimicrobials are in development.

Human and Economic Cost

Prevalence of AMR puts an economic strain on the healthcare system and countries because of prolonged hospital stays, increased treatment costs, and decreased productivity [65]. MDR bacterial infections have been correlated with costs in the region of billions of dollars per year. Specifically, infections caused by *S. aureus*, *E. coli, K. pneumoniae*, *A. baumanii,* and *P. aeruginosa* added up to $0.5 billion and $2.9 billion in Thailand and the US, respectively [66]. These numbers do not take into consideration direct healthcare costs that could go up to $20 billion in the US, and the $35 billion in loss of productivity annually, according to the Centre for Disease Control and Prevention (CDC) [65,67]. Additionally, the annual cost of AMR in Europe is estimated at €9 billion [65].

The consequences may be more pronounced in developing countries. It is predicted that they may see annual losses of 5-7% in their GDP, equating to $100-210 trillion [65,68]. Eventually, it would worsen the already big economic gap between the developed and developing world, driving them to deeper poverty and inequality.

Another affected sector would be global trade. Transfer of food and other perishable goods would be hindered due to higher safety measures and spoilage by foodborne pathogens [69].

Morbidity and mortality rates are already devastating. Each year in the U.S., at least 2.8 million people are infected with antibiotic-resistant bacteria or fungi, resulting in more than 35,000 deaths [70]. In 2017, MDR tuberculosis was the leading cause of death among AMR pathogens, killing approximately 250,000 people [71]. Future projections are not favourable. It is estimated that by 2050, the leading cause of death would be MDR infections, surpassing cancer and diabetes deaths combined [72].

Much of the conversation around AMR is focused on bacterial infections whilst fungi-associated diseases are neglected. Three classes of antifungal drugs are in clinical use. Azoles and polyenes were introduced 40 years ago, while echinocandins have only been employed for less than a decade [73]. Scarcity in novel

antifungal therapies has led to resistance development by the most common causative agents [73,74]. The mortality rate for the three most common species of human fungal pathogens are *Candida albicans*, 20%–40%; *Aspergillus fumigatus*, 50%–90%; and *Cryptococcus neoformans*, 20%–70% [75–77]. These findings underlie the equal importance of fungal and bacterial MDR infections.

Strategies to combat AMR

AMR afflicts everyone regardless of age or ethnicity. Measures to counteract it should be taken on national and international level. Surveillance of antibiotic consumption and supply chains improved medical infrastructure, strict sanitisation rules, proactive detection of resistance in livestock and humans, as well as introduction of courses on AMR and spread for medical personnel are a few actions to be considered. Countries which implemented such strategies have successfully decrease AMR presence. [52,78]. One example is that of MRSA and its reduction from endemic to sporadic in the UK [52,79]. According to a CDC report in 2020, MDR *P. aeruginosa* infections dropped by 30%, from 46,000 to 32,600 cases, and vancomycin-resistant *Enterococcus* cases also showed a diminishing trend [70].

However, more actions are needed if we are to reverse the AMR crisis. Policymakers should collaborate with academics for informing and establishing health guidelines. The private sector should be incentivised in contributing more intensely to the antibiotic pipeline. Both the European Union and the UK have considered financial strategies on stimulating pharmaceutical companies to re-enter antibiotic research [80,81]. Countries could individually or in collaboration invest in developing diagnostic tools and surveillance systems aiming for the prevention of epidemics and outbreaks. The Global Antimicrobial Resistance Surveillance System (GLASS) collects data with standardised methods, on critical human pathogens worldwide in order to monitor AMR trends. Moreover, the public should be educated on the correct use of antimicrobials and improved hygienic habits.

On an international scale, a collaboration among governments, academia, national and international organisations, and pharmaceuticals could aid in curbing the AMR threat. Such collaborations are exemplified by the Global Antibiotic Research and Development Partnership (GARDP). GARDP is a joint

initiative of WHO and Drugs for Neglected Diseases initiative (DNDi) dedicated in supporting R&D through public-private partnerships and assuring sustainable, affordable access to treatments. Likewise, IACG aims to bridge international organisations and individuals for generating a combat strategy against AMR.

R&D has focused on a variety of antimicrobial strategies. One of the main approaches is the modification of existing antibiotic compounds creating semisynthetic or fully synthetic molecules. These molecules exhibit enhanced pharmacological properties in comparison to the natural counterparts [82]. A proposed alternative approach is the design of "predrugs" which are initially inactive compounds until they are metabolised by a bacterium-specific enzyme and exert their antimicrobial activity intracellularly [35]. Additionally, species-specific antibiotics have made their way in the fight against pathogens, such as *M. tuberculosis* [35].

Although new antibiotic classes are identified [83], the pace of discovery has significantly declined in the past decades [35]. This bottleneck is exacerbated by the inability of antibiotics to penetrate the bacterial cell wall in order to reach their cytoplasmic target. Recently, WHO published a list of high priority pathogens in order to encourage R&D towards these MDR organisms. The category of critical pathogens includes carbapenem-resistant *A. baumannii,* carbapenem-resistant *P. aeruginosa*, and carbapenem-resistant ESBL-producing *Enterobacteriaceae.* The list emphasises the imminent threat of MDR Gram-negative bacteria and the urgent need to develop new antibacterial strategies. Many classes of antibiotics perturb Gram-negative bacterial cell wall metabolism but resistance has eventually been developed [43,84,85]. The cell wall of Gram-negative bacteria is comprised of three layers: the outer membrane (OM), the inner membrane (IM), and the peptidoglycan (PG) layer in between. Studying the bacterial cell-wall could promise to reveal novel antibiotic targets. The first rotation examined the regulation of *E. coli* PG amidases by two regulatory proteins, YraP and NlpI. Amidases are hydrolytic enzymes crucial for PG separation during cell division. Dysregulation of these enzymes could compromise cell wall integrity and lead to cell lysis.

Significant contributions towards AMR surveillance and control were made by the introduction of NGS technologies. The low-cost and availability of a

variety of tools for analysing whole genome sequencing data have allowed their implementation in clinical applications, such as investigation of outbreaks in nosocomial environments [86,87]. The third chapter showcases how to perform a bioinformatics analysis on NGS data, from *de novo* assembling to extracting information on ARGs presence and phylogenetic inferences.

While many antibiotics primarily target essential metabolic pathways, other unconventional strategies prioritise the preclusion of non-essential functions for bacterial survival. Examples consist of virulence attenuation and biofilm formation inhibition which could impede the establishment and progression of infection [88–91]. The rationale behind this is the selective pressure to develop resistance would not be as strong as that for current antibiotics, leading to lower chances of developing resistance [91]. Many of the virulence factors of *P. aeruginosa* are under the control of quorum sensing (QS) regulatory mechanisms [92]. *P. aeruginosa* possesses three QS systems with one of them being specific to the species, the *pqs* system. The *pqs* system regulates the expression of virulence factors including pyocyanin production and biofilm formation among others [93]. For this reason, it has been the focus of antivirulent drugs against *P. aeruginosa* [94,95]. The final chapter of this thesis discusses a recently identified regulator of *pqs*, a small non-coding RNA (sRNA) named PqsX, and its potential roles in the *pqs* regulatory mechanism. Additionally, it explores how the study of PqsX could progress on to a PhD project.

Chapter 2: Investigating the regulation of septal peptidoglycan separation in *E. coli*

Abstract

Cell division in Gram-negative bacteria necessitates split of the PG layer by hydrolytic enzymes. These enzymes are tightly controlled in order to maintain cell wall integrity. Past research in *E. coli* has focused on amidase activation by EnvC and NlpD membrane proteins however little is known of other regulators involved. The purpose of this study was to investigate the regulation of amidases by two new OM lipoproteins, NlpI and YraP. Firstly, soluble variants of the amidases and their activators EnvC and NlpD were purified. Pull-down assays were performed in order to demonstrate interactions between YraP and the purified proteins but proved inconclusive. Moreover, *in vitro* PG hydrolysis assays were conducted to show whether NlpI or YraP alters amidase activity which revealed that NlpI does not participate in AmiA hydrolytic activity. Overall, this project is a preliminary study of the involvement of YraP and NlpI in the regulation of PG cleavage during cytokinesis, providing the basis for further research on the topic.

Significance Statement

The peptidoglycan sacculus has been an attractive antibacterial target with a plethora of antibiotics, interfering with its metabolism. However, the mode of action of many envelope targeting drugs is still not fully understood. Therefore, this project aims to gain a deeper understanding of PG regulation and metabolism as this may help reveal unknown antibacterial targets and facilitate knowledge on the mode of action of envelope targeting antibiotics.

Introduction

Gram-negative bacteria are enclosed by a three-layered cell envelope comprised of the OM, the IM, and the PG layer lying in between. PG sacculus is a mesh-like network made of polysaccharide chains cross-linked by short stem peptides completely enclosing the IM (fig. 4). PG is responsible for cell shape maintenance

and osmotic pressure resistance [96], thus disturbance of its biosynthesis during cell division or growth potentiates cell lysis. Cell wall growth is a dynamic process meaning that new chains are constantly added, and old ones are removed [97]. Addition of new material is executed by PG synthases called penicillin-binding proteins while extraction of PG is carried out by hydrolytic enzymes belonging in four categories: lytic transglycosylases, endopeptidases, carboxypeptidases, and amidases. Septal PG thickens between daughter cells prior to its careful split in coordination with the invagination of the two membranes. Precise regulation of PG remodelling is vital to allow for cell separation without causing breaches that can lead to cell lysis [98]. Responsible for this is the divisome, a multiprotein complex assembled at the division site [99]. The tubulin-like FtsZ protein is polymerised into a ring-like structure, the Z-ring, which acts as a scaffold for the recruitment of the remaining division proteins [100] (fig. 4). Thus synthases, hydrolases, and their regulators come in proximity facilitating spatiotemporal control over their activities.

In *E. coli*, amidases possess the central role of septal PG separation [97,101]. They cleave the bond between a stem peptide and a glycan monomer resulting in breaking crosslinks between the polysaccharide chains (fig. 4). There are three amidases: AmiA, AmiB, and AmiC, all bearing a LytC-type *N*-acetylmuramyl-*L*-alanine amidase domain and are zinc-dependent [102]. Except for AmiA which is peripherally localised, AmiB and AmiC are located at the division site [103]. They are partially redundant and deletion of one or two amidases does not cause severe problems in PG biosynthesis [97]. However, a triple mutant produces long cell chains with a thick septal PG layer between the cells [104]. Moreover, their autoinhibitory nature requires an activator for them to function and couples their activation to the assembly of the cytokinetic ring [98]. AmiA and AmiB are activated by the IM associated EnvC and AmiC by the OM lipoprotein NlpD [98]. Both activators possess a degenerate LytM metalloendopeptidase domain and probably possess more functions during division, as EnvC may stabilise the divisome and NlpD causes OM defects independently of AmiC [98,105].

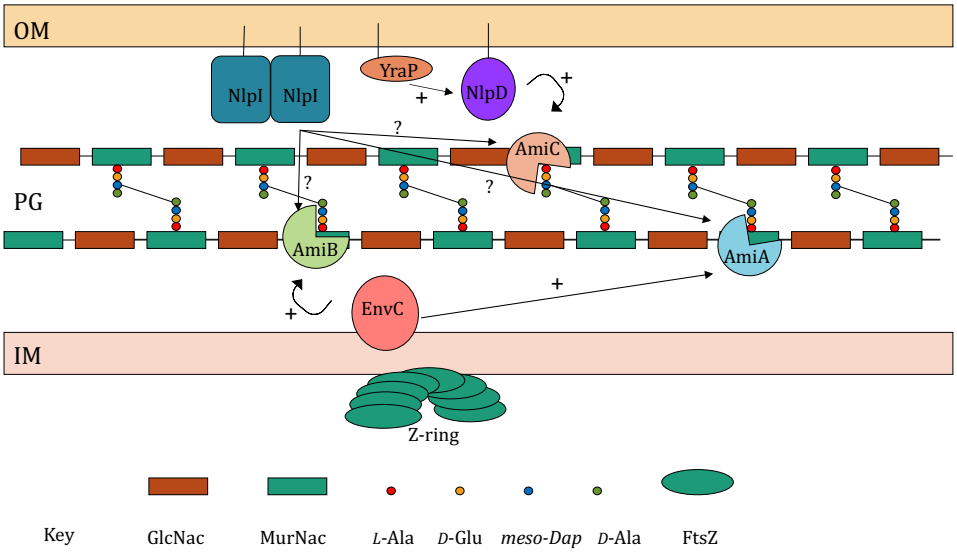

Figure 4. Chemical structure of PG and protein localisation. Gram-negative bacteria possess a three-layered envelope consisted of the OM, the PG, and the IM. The PG is a matrix made of polysaccharide chains. Each PG chain is a series of alternated *N*-acetylglucosamine (GlcNAc) and *N*-acetylmuramic acid (MurNAc) saccharides. The chains are crosslinked via short peptides which are bound to MurNAc. The amidases exhibit periplasmic localisation and cleave the bond between the stem peptide and MurNAc thereby breaking the links between two polysaccharide chains. AmiA and AmiB are activated by the IM-associated protein EnvC. YraP, an OM lipoprotein of unknown function, is thought to activate NlpD, the regulator of AmiC, but its plausible relation to the other amidases has not yet been explored. The lipoprotein NlpI forms homodimers which act as general adaptor for PG hydrolases. It was previously showed that NlpI deletion affects the abundance and stability of amidases. However, there are no available data on how NlpI regulates amidase activity.

Previous research suggested that NlpD is activated by YraP, a non-essential OM lipoprotein of unknown function [105]. YraP has two BON (bacterial OsmY nodulation) domains, its deletion causes OM defects and it is localised independently of NlpD and AmiC [105]. However, there are no *in vitro* or *in vivo* evidence of it regulating NlpD.

Another non-essential protein was proposed recently to be implicated in PG regulation. NlpI, a predicted OM lipoprotein, is known for targeting the endopeptidase MepS for degradation [106]. NlpI appears to be a general adaptor for PG biosynthetic enzymes, contributing in both cell elongation and division [107]. It forms homodimers and each monomer bears two tetratricopeptide helix-turn-helix (HTH) domains, as well as two non-canonical TPR motifs commonly found

in protein-interacting peptides [108,109]. Two-dimensional Thermal Proteome Profiling (2D-TPP) assay revealed that in a Δ*nlpI* mutant, major PG proteins changed in abundance and thermostability [107] with amidases levels falling and NlpD and YraP becoming unstable, reflecting the pleiotropic effect of *nlpI* deletion [107]. Additionally, it was showed that when immobilised NlpI was incubated with detergent-solubilised membrane proteins of *E. coli* under high salt binding conditions, NlpI was able to retain both EnvC and AmiA among other divisome proteins which suggested strong interactions *in vitro* [107]. When taken together, these results imply that NlpI may play a role in amidase regulation.

Here, the role of NlpI and YraP as putative regulators of amidase activity during cell wall division was investigated. Assuming the plausible activation of NlpD by YraP, pull-down assays were performed to demonstrate a direct interaction and also between YraP and the other purified proteins. The rationale behind this was that YraP may play a broader role than initially thought. Finally, *in vitro* PG degradation assays were employed to explore the participation of YraP and NlpI in amidase hydrolytic activity.

Materials and Methods

Strains and plasmids

E. coli BL21(λDE3) strain was used for protein overexpression. The strains were cultured in LB with appropriate antibiotics (50 μg/mL carbenicillin, 25 μg/mL kanamycin. H-SUMO-AmiB/AmiC/AmiA/NlpD were purified from BL21(λDE3) carrying respective plasmids pTB324//pTU203/pTB327/pTU119. EnvC was purified from MB1 plasmid.

Transformation

Plasmids were introduced into BL21 through chemical transformation as described in Sambrook, Joseph. Molecular Cloning: a Laboratory Manual. Cold Spring Harbor, N.Y. :Cold Spring Harbor Laboratory Press, 2001.

Purification

Protein purification was carried out as described in [98] with a few alterations. All proteins were missing their signal peptide for targeting to the cell envelope and

therefore were produced as cytoplasmic soluble variants. All proteins were overproduced with a 6xhis-SUMO tag fused to their N-termini apart from EnvC, which was fused to an uncleavable his-tag.

Overnight cultures were diluted 1:1000 in LB with the appropriate antibiotics and were incubated at 37°C until OD_{600} = 0.4. Afterwards, IPTG was added in the cultures to a final concentration of 1 mM and incubation was continued for four more hours. Cells were harvested by centrifugation at 15,970 x g, 15', at 4°C, and were stored in -30°C until needed for protein purification. The cells were resuspended in buffer A (300 mM NaCl, 50 mM Tris-HCl pH 8, 10% v/v glycerol) with 20 mM imidazole and protease inhibitor (Sigma-Aldrich). Cell disruption was done using a high-pressure homogenizer (C3 EmulsiFlex, Avestin) at 15,000 psi. Cell debris were pelleted by centrifugation at 48,384 x g, 1 h, at 4°C. Proteins were incubated on Ni^{2+} Nta agarose beads (Qiagen) in silica columns and then eluted with buffer A containing 300 mM imidazole.

Next, all proteins were dialysed against buffer A and cleaved by the 6xhis tagged SUMO protease (H-SP) overnight at 4°C. Both cleaved SUMO and H-SP were removed from the solution by a second step purification with Ni^{2+} Nta beads. In the case of AmiA, second step purification was performed with Co^{2+} Nta beads. All proteins were stored in buffer A at -30°C. EnvC was dialysed against and stored in buffer B (150 mM NaCl, 50 mM Tris-HCl pH 8, 10% v/v glycerol) without his-tag cleavage. Protein concentration was measured with the DS-11 Spectrophotometer, DeNovix Inc.

Nickel cobalt exchange

Cobalt beads were generated by striping nickel from Ni^{2+}Nta beads and replacing it with cobalt following the protocol"Reuse Ni^{2+} Nta resin" from Qiaexpressionist Handbook: https://www.qiagen.com/mx/resources/resourcedetail?id=79ca2f7d-42fe-4d62-8676-4cfa948c9435&lang=en. The only change was the use of 100 mM $CoCl_2$ in place of 100 mM $NiSO_4$.

SDS-PAGE gel electrophoresis

Protein samples were diluted 1:1 in SDS buffer (50 mM Tris-HCl, pH 6.8, 2% w/v SDS, 10% v/v glycerol, 0.02% w/v bromophenol blue, 10% v/v β-

mercaptoethanol and boiled for 10 minutes. Next, samples were loaded on 12% w/v SDS polyacrylamide gels, prior to staining with Coomassie brilliant blue (0.4 M citric acid, 20% v/v isopropanol, 0.2% w/v Coomassie Brilliant blue-R250). Staining was performed by microwaving gels for 30 seconds, allowing five minutes incubation before repetitive cycles of destaining with water and microwaving.

Ni^{2+} Nta Pull-down assays

Essentially, a pair of proteins, one with an attached his-tag (bait) and one without (prey), was incubated on metal-ion beads. If the proteins interact, the his-tagged protein will retain the non-his-tagged protein to the beads and will be eluted together. If not, then only the his-tagged protein will be detected. Agarose beads were preequilibrated in buffer C (50 mM NaCl, 50 mM Tris pH 7.5). His-tagged proteins were incubated with untagged proteins in equimolar concentrations (5 μM) for five minutes at room temperature. Subsequent washes with buffer C followed and the retained proteins were eluted by addition of SDS and boiling for 10 minutes.

Peptidoglycan Degradation assays

Assays of 100 μL volume were carried out in buffer C (150 mM NaCl, 50 mM Tris-HCl pH 7.5) with the addition of FITC labelled peptidoglycan sacculi to a final concentration of 1 mg/mL. Protein concentration is indicated below figures. Reactions were executed in a benchtop Eppendorf ThermoMixer at 37^{o}C, 1000 rpm for an hour, unless stated otherwise, before termination via filtration. Since FITC absorbance is pH-sensitive, 50 μL 0.5 M NaOH were added to each sample to adjust the pH. Samples were excited at 485 nm and emission was measured at 520 nm. The fluorescence of the negative control (no enzyme was added) was subtracted as background signal. Then, hydrolytic activity was measured as percentages of fluorescence value of a sample divided by the value of lysozyme sample (positive control). To measure hydrolase activity in presence of zinc, $ZnCl_2$ was added in a final concentration of 0.05 mM.

Results

Protein purification

To investigate protein-protein interaction between the amidases and the potential regulators, the first step was to purify the proteins of interest: AmiA, AmiB, AmiC, NlpD, and EnvC (table 2). YraP and NlpI have been previously isolated. The protocol from [98] was used with some modifications. More adjustments were required for the purification of AmiA because of the non-specific binding of AmiA to the nickel beads (fig. 5A). To resolve this problem, the protein was eluted by adding a low concentration of imidazole, as was suggested in the published method, and incubating it with the resin for less time but without success. Our next action was to change the metal ion of the resin, from nickel to cobalt, which has a weaker affinity for his-tag and histidine-rich proteins. The protocol for recharging agarose beads was utilised and AmiA bound less strongly to the beads and was eventually purified with the minimum amount of SUMO present (fig. 5B). In conclusion, the protocols for purifying all proteins were established, and all purified proteins are illustrated in figure 5C.

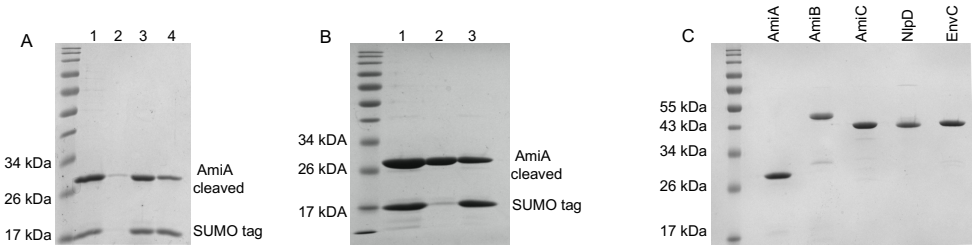

Figure 5. Successful purification of amidases and their regulators. A) AmiA purification with nickel beads. After SUMO cleavage, there was free SUMO tag and cleaved AmiA in the solution (lane 1). During the second purification, cleaved AmiA should have flowed through the nickel beads without binding on them however there was only a slight amount of AmiA in the flow-through solution (lane 2). AmiA was retained on the nickel beads and was eluted along with the cleaved SUMO tag in presence of 50 mM (lane 3) and 100 mM (lane 4) imidazole. B) AmiA purification with cobalt beads. After SUMO cleavage (lane 1), AmiA was present in satisfactory quantities in the flow-through solution without SUMO contamination (lane 2). Nevertheless, AmiA maintained affinity for the cobalt beads as well, since it was also present in the elution step with 200 mM imidazole (lane 3). C) All proteins purified in the present study. All proteins used in subsequent experiments did not bear SUMO-tag except for EnvC, which had an uncleavable his-tag.

Protein	Function	Localisation	Predicted MW (kDa)	Predicted MW without signal peptide (kDa)
AmiA	Amidase	Periplasm	31.41	27.84
AmiB	Amidase	Periplasm	47.98	45.48
AmiC	Amidase	Periplasm	45.63	42.40
NlpD	Activator of AmiC	OM lipoprotein	40.15	37.55
EnvC	Activator of AmiA and AmiB	IM	45.60	43.94
NlpI	General adaptor protein	OM lipoprotein	33.62	31.52
YraP	Unknown	OM	20.03	18.11

Table 2. Proteins studied in the current project. All proteins were isolated without their N-terminal signal peptide.

YraP protein interaction assays

Having purified all necessary proteins, protein interaction assays were performed. Because YraP is probably implicated in the activation of NlpD and the regulation of PG separation during cell division, it was investigated whether there is a direct interaction between YraP and all purified proteins, as well as NlpI, by performing pull-down assays.

YraP bearing his-tag was incubated with either AmiB or AmiC (fig. 6A). AmiA was not included due to its non-specific interactions with the resin. Both amidases had affinity for nickel beads, hence the bait-prey relation was switched such that the amidases bore the his-tag and YraP was without (figure 6B). It seemed that cleaved YraP deteriorated faster than the non-cleaved variant despite being stored under the same conditions, rendering the use of cleaved YraP impractical. Non-specific binding was also observed when freshly prepared cleaved YraP was used, as a result the pairs YraP-NlpI and YraP-EnvC were not tested. Another way to reduce non-specific interactions was by refining the incubation buffer. Salt concentration was tripled to reduce weak protein interactions, or a low concentration of imidazole was added. As can be seen in figures 6C and D, neither of these alterations had any effect.

Lastly, pull-downs were conducted with cobalt beads instead of nickel beads. By testing the amidases and NlpD alone, non-specific binding by all proteins

was detected. Nonetheless, it is a comparative assay which means the controls and the eluted pairs are compared for increased band intensity. Comparison between the control and the eluted bands revealed no apparent rise in the band intensity of the prey, implying no interaction between the tested combinations. These data suggest that pull-down experiments are not suitable for analysing these protein interactions.

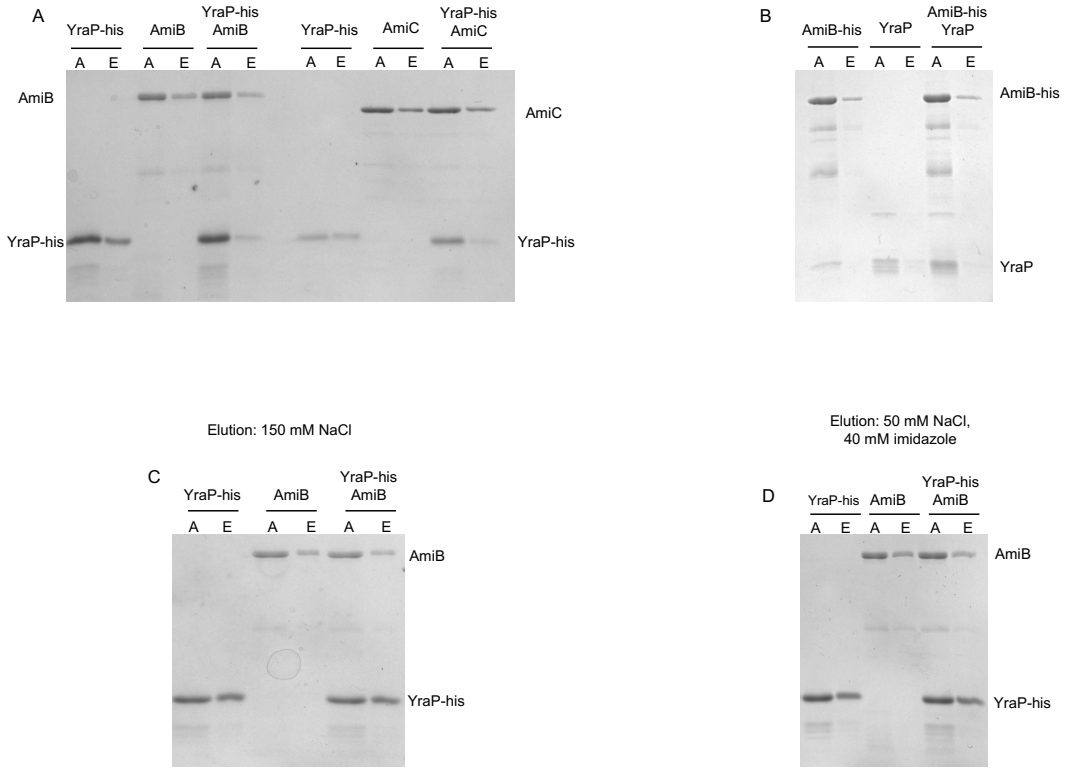

Figure 6. *in vitro* protein interactions between YraP and amidases by pull-down assays. Incubation of each protein was done on Ni^{2+}-NTA beads either together or alone. Detection of non-his-tagged protein in presence of the his-tag protein indicated physical interaction. A) YraP-AmiB and YraP-AmiC pull-down. Non-tagged AmiB and AmiC were retained on the beads without presence of YraP which showed non-specific interaction with the beads. B) AmiB-his and YraP pull-down. Existence of multiple faint YraP bands instead of one intense band points to protein degradation, so non-his tagged YraP could not be used. The rest of the bands are impurities left after the first purification step. C) YraP-his and AmiB pull-down in 150 mM NaCl incubation buffer. Non-tagged AmiB was retained on the beads without presence of YraP which showed non-specific interaction with the beads. D) YraP-his and AmiB pull-down in 50 mM NaCl and 40 mM imidazole incubation buffer. Non-tagged AmiB was retained on the beads without presence of YraP which showed non-specific interaction with the beads. A: applied, E: eluted.

Assessment of NlpI and YraP effect on amidase activity in vitro

Next, the participation of NlpI and YraP in amidase activity regulation was explored since NlpI can interact with some of the amidases and their activators [107], as well as YraP is associated with NlpD activation [105]. PG hydrolytic assays were conducted *in vitro*, with the enzyme concentrations and assay duration being based on the methods of Uehara *et al.* (2010). The PG sacculi used here had the fluorophore FITC attached to them and assays were terminated by filtration. Essentially, amidases activated by their regulators would digest the PG releasing FITC in the solution which could be measured after filtration. The activity was then expressed as the percentage of the fluorescence signal of each sample relative to lysozyme activity (positive control).

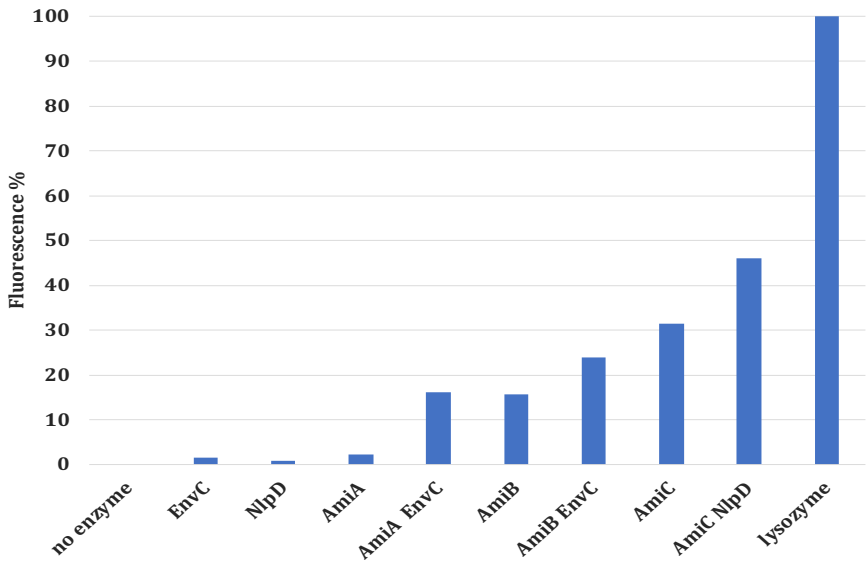

Figure 7. Measuring hydrolytic activity of amidases by *in vitro* PG hydrolytic assays. FITC-labelled PG sacculi after amidase digestion would release FITC in the solution relative to their hydrolytic activity. Amidase activity is expressed as the percentage of the detected fluorescence signal to the lysozyme signal (positive control) after subtracting background signal of the negative control (no enzyme). Enzyme concentrations: AmiA, 1 µM; AmiB, 2 µM; AmiC, 2 µM; EnvC, 1 µM; NlpD, 2 µM. Assays were carried out for 16 h, at 300 rpm. The activity of all amidases is increased in presence of their cognate activator, in a similar fashion to the results from Uehara *et al.* (2010). The results were obtained from one experiment.

The first step was to replicate the results from Uehara *et al.* (2010) which revealed similar amidase activity increase. (fig. 7). Secondly, knowing that amidases are zinc-dependent and addition of zinc in a PG degradation assay with AmiA increased its activity [102], it was tested whether the addition of zinc could enhance the activity of AmiA (fig. 8A). Contrary to expectations, the fluorescent signal was reduced, pointing to the probability of zinc quenching FITC signal. Therefore, a series of FITC dilutions in the presence or absence of zinc was performed. Figure 8B illustrates that zinc did not affect fluorescence signal. Since there was not a satisfactory explanation of why amidase activity appeared lower with zinc, zinc was omitted from the following assays.

Afterwards, the ability of NlpI to alter amidase activity was tested. It revealed that NlpI probably did not affect AmiA and AmiC activity, but it could negatively impact AmiB because the activity of AmiB was reduced almost by half in presence of NlpI (fig. 9A). Subsequent experiments with AmiA and increasing concentrations of NlpI demonstrated that NlpI did not change AmiA activity despite their previously reported *in vitro* interaction (fig. 9B) [107]. Due to lack of time, AmiB and AmiC assays, as well as the respective YraP experiments were not conducted. Taken together, these results indicate that NlpI might not be essential in amidase activation.

Discussion

Separation of PG layer between daughter cells is a vital process during cell division in Gram-negative bacteria. However, the regulatory mechanisms surrounding it remain to be elucidated. The aim of this investigation was to assess the involvement of two new factors, NlpI and YraP, in the regulation of amidases in septal cell wall remodelling. To this end, soluble variants of the amidases AmiA, AmiB, AmiC and their activators NlpD and EnvC were purified. Difficulties on cleaning AmiA from the cleaved SUMO tag arose due to affinity for the nickel beads which were overcome by changing them for cobalt beads.

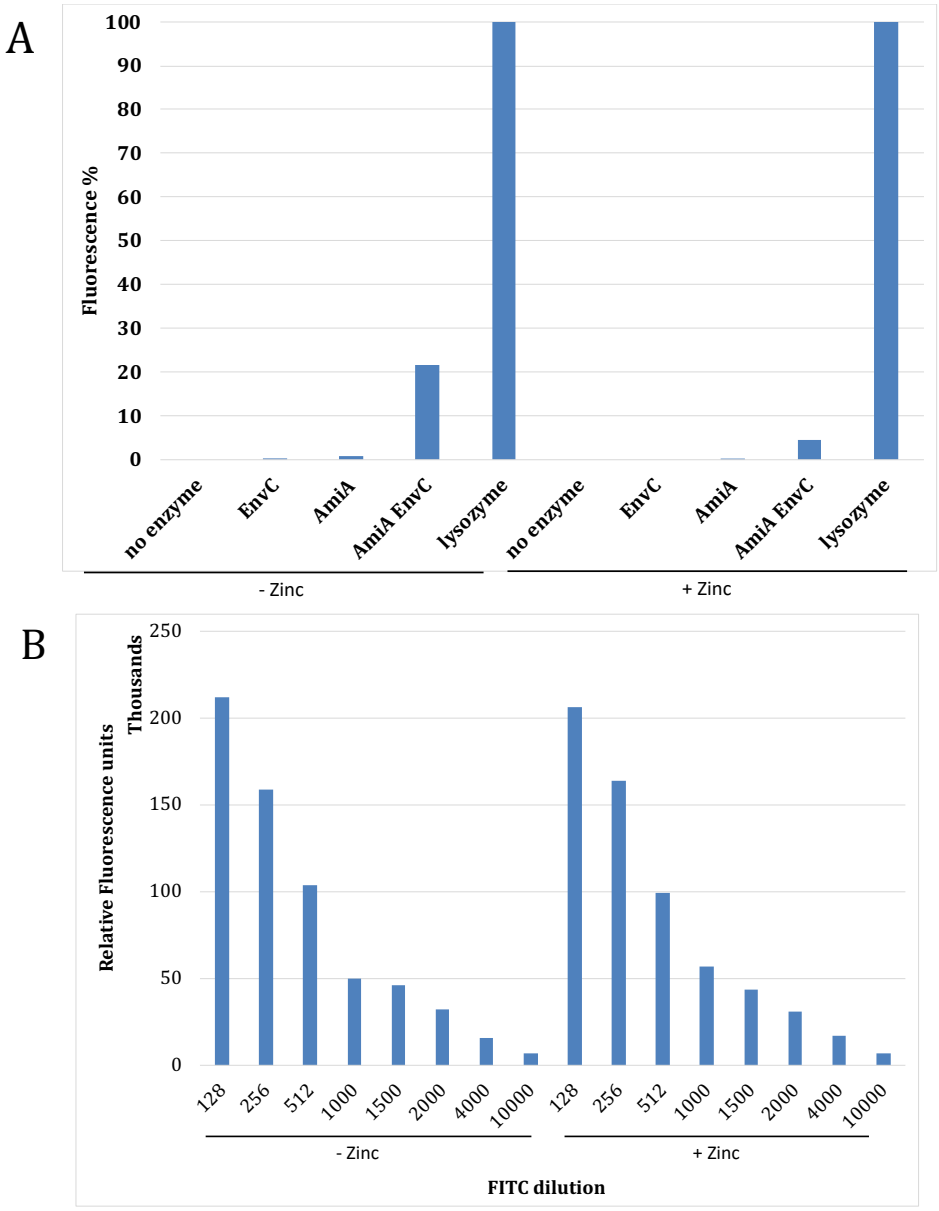

Figure 8. Assessing zinc effect on amidase activity. A) Reduction in AmiA activity in presence of zinc in *in vitro* PG degradation assays. FITC-labelled PG sacculi after amidase digestion would release FITC in the solution relative to their hydrolytic activity. Amidase activity is expressed as the percentage of the detected fluorescence signal to the lysozyme signal (positive control) after subtracting background signal of the negative control (no enzyme). When zinc was in the buffer, the hydrolytic activity of AmiA decreased compared to no addition of zinc. Protein concentration: AmiA, 2 μM; EnvC 1 μM. B) FITC fluorescence signal in presence of zinc. In serial dilutions of 100 μM FITC, zinc was added to a final concentration of 0.05 mM and samples were incubated for 5' at room temperature, before terminating the reaction with addition of NaOH. The fluorescent signal was not altered regardless of zinc which indicated that the metal ion might not quench FITC. Numbers on horizontal axis indicate FITC dilution and on vertical axis are the relative fluorescence units in thousands.

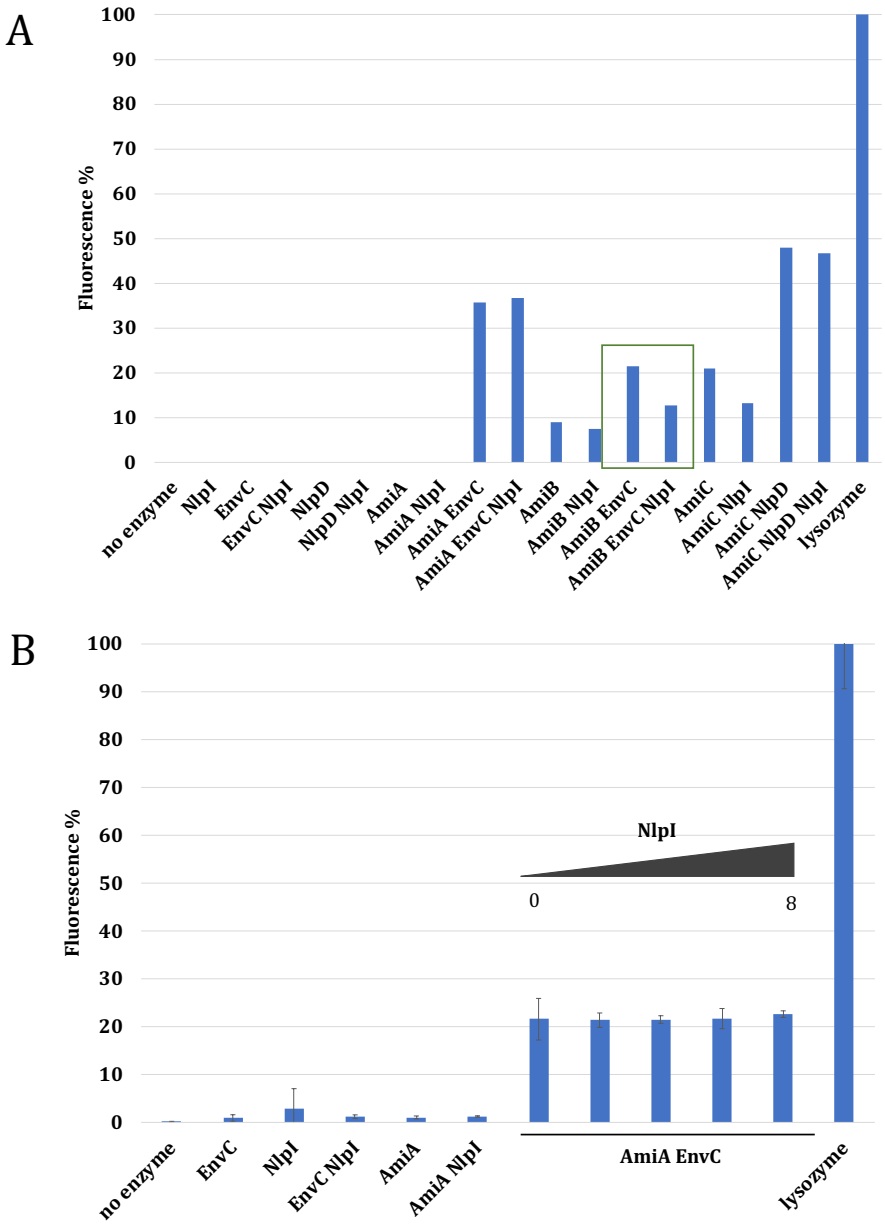

Figure 9. Measuring hydrolytic activity of amidases in presence of NlpI by *in vitro* PG hydrolytic assays. FITC-labelled PG sacculi after amidase digestion would release FITC in the solution relative to their hydrolytic activity. Amidase activity is expressed as the percentage of the detected fluorescence signal to the lysozyme signal (positive control) after subtracting background signal of the negative control (no enzyme). A) Hydrolytic activity of all amidases with or without addition of NlpI. The activity of AmiA and AmiC do not seem to be affected by NlpI when their activators are present. On the other hand, AmiB activity is reduced (green box). Data were obtained from one experiment only. Enzyme concentrations: AmiA, 1 µM; AmiB, 2 µM; AmiC, 2 µM; EnvC, 1 µM; NlpD, 2 µM; NlpI, 2µM.: B) Hydrolytic activity of AmiA in presence of NlpI concentration gradient, from 1 to 8 µM. AmiA hydrolytic activity remained stable despite the increasing concentrations of NlpI. Enzyme concentrations: AmiA, 2 µM; EnvC, 1 µM; NlpI, 1 µM, 2 µM, 4 µM, and 8 µM. The results are average of three independent reactions. Error bars display standard deviation.

After protein purification, direct protein interactions between YraP and the rest of the proteins were investigated. Pull-down assays could not safely infer any protein interactions because of non-specific binding to the beads. All amidases and NlpD bear metal-binding residues [98,102] which could be the reason for this problem, additionally explaining the purification difficulties that occurred earlier. Notwithstanding this limitation, the results suggested that maybe YraP does not interact with the tested proteins. If this is true, then YraP might not be implicated in the amidase regulation and NlpD activation, as was previously proposed [105]. However, another experimental approach, such as MST (MicroScale Thermophoresis) [110], may shed light on this hypothesis. In fact, preliminary MST results of another student indicated binding of YraP to NlpI.

In MST, an infrared beam generates temperature gradient, in which the movement of a fluorescence-producing molecule is quantified [110]. MST is based on the phenomenon of thermophoresis, the directed movement of molecules in a temperature gradient. It is a highly sensitive approach for inferring molecule interactions because the movement is affected by the interface between the molecule and the solvent; the shape, charge, and conformation of the molecule [110]. As a result, any small change, such as protein-protein binding, can be detected [110].

NlpI is proposed to act as a protein scaffold, bringing physically close several different proteins at the division site [107]. Consequently, NlpI may not exert direct control on the activities of the enzymes but may facilitate the interaction with regulatory proteins that otherwise would be impossible. Such a suggestion is on par with the NlpD activation model proposed by Tsang *et al* (2017). The authors suggested that YraP may directly or indirectly activate NlpD during envelope constriction. Considering that YraP has not been showed to interact with NlpD yet, it may do so through its interaction with NlpI. To investigate this suggestion, a three-protein MST could be conducted in which NlpD may bind to YraP only in the presence of NlpI.

YraP regulation mediated by NlpI can also explain the absence of AmiA activity change in the presence of NlpI demonstrated in the second part of the project. The results also indicated that NlpI may negatively control AmiB, but more experiments are needed to statistically verify this observation. Even though NlpI interacted *in vitro* with some of the amidases [107], it could be plausible that the

interaction with AmiA and EnvC was mediated by other proteins that directly interacted with NlpI. Another explanation could be that the cooperation of YraP and NlpI might be one of the regulatory forces behind envelope constriction instead of each protein alone. A natural progression of this work would be to do the amidase activity assays in the presence of YraP and, both YraP and NlpI. In this way, it could be demonstrated whether the cooperation of these two can regulate amidases or at least NlpD. Additionally, it could reveal a more general role for YraP outside of NlpD activation. The present study has provided insights into the regulatory machinery of cell envelope reconstruction at the division site which can aid in identifying antibiotic targets against pathogenic Gram-negative bacteria.

Chapter 3: Bioinformatics Project

Abstract

Technological progress has enabled the generation of massive amounts of biological data transforming the field of AMR control and surveillance. Next Generation Sequencing (NGS) has been widely deployed in the investigation of hospital outbreaks and the genetic characterisation of the causal pathogens. A variety of tools can be used to assemble NGS data and analyse them for the existence of ARGs and virulence factors or construct a phylogenetic analysis. In this project, publicly available raw sequence data were *de novo* assembled and annotated. Then, they were analysed for the presence of AMR determinants and phylogenetic trees were created using three different approaches.

Introduction

The technological advancement in DNA sequencing has revolutionised the area of AMR control and surveillance. The availability and low cost of NGS enabled typing of pathogenic bacterial strains, molecular epidemiology, and pathogenomics [111]. Based on this information, controlling measures of outbreaks or spread of AMR are shaped and implemented in a local and global scale. However, data generation has outpaced their meaningful interpretation and the choice of computational tools can affect the research outcome.

In this project, raw sequence reads were *de novo* assembled and annotated. Then, they were analysed for presence of ARGs and Genomic Islands (GIs), as well as used to construct phylogenetic trees utilising different phylogenetic pipelines. The aim of the project was to compare the results of the present research to those of the publication from which the sequence reads were obtained. The raw data were publicly available and were initially analysed in the paper "Genomic characterization of a local epidemic *P. aeruginosa* reveals specific features of the widespread clone ST395" [112].

P. aeruginosa is a Gram-negative opportunistic pathogen able to survive in a plethora of environmental habitats. It is associated with antimicrobial resistant infections in nosocomial environments; causes a wide variety of human diseases;

and is responsible for high morbidity and mortality in Cystic Fibrosis (CF) patients [113,114]. A few sequence types (STs) of *P. aeruginosa* have been disseminated in a global scale despite its non-clonal population structure [115]. The genomic and structural characteristics of these clones which have aided their prevalence have not been determined yet. One of these clones is ST395, which has infected approximately 300 patients in the University Hospital of Besançon (Besançon, France) in an eleven-year period [116]. It was also speculated that a ST395 strain had transmitted through the plumbing system in the wards of burn patients in the University Hospital of Birmingham [117]. In the paper described here, the authors investigated what features of the global ST395 clone have assisted to establishing outbreaks in French and British hospitals.

The pathogenesis of *P. aeruginosa* is attributed to its large genome (over 6 Mbp) carrying a rich arsenal of virulence factors and the ability to form antibiotic-resistant biofilms [118,92,119]. The core genome is estimated in the area of 5,200 genes (90% of all genes in the genome) and the pangenome at 9,300 [119,120]. Many of the accessory genes are harboured in mobile genetic elements, such as GIs and integrative conjugative elements (ICEs) of clinical or environmental origin [119–121]. A considerable number of ARGs are part of the core genome of the species providing intrinsic resistance to a diverse set of antibiotics. Some of these genes are the *ampC* gene of cephalosporinase and those encoding for fluoroquinolone resistance [119].

Petitjean *et al.* sought to identify the genetic characteristics that enabled the distribution and persistence of ST395 in hospital settings. They sequenced and studied the genomic features of DHS01, an isolate responsible for a hospital outbreak in France. Their main focus was on the ARGs, virulence genes and mobile genetic elements that were shared only between DHS01 and a set of ST395 isolates from outbreaks in other hospitals.

Materials and Methods

Sequence retrieval and genome assembly

The two datasets analysed here were: dataset 1, which included the sequences of 10 non-ST395 isolates and the 12 ST395 isolates; and dataset 2 included the 82

complete genomes of *P.* aeruginosa deposited in GenBank until July 2017. The raw sequence data were retrieved from the bioprojects PRJNA379554 (https://www.ncbi.nlm.nih.gov/bioproject/?term=PRJNA379554) and PRJNA380885 (https://www.ncbi.nlm.nih.gov/bioproject/?term=PRJNA380885). The sequence of PT_F, the ST395 isolate from Birmingham, was downloaded from European Nucleotide Archive (ENA), and the sequences of PAO1 and the rest of *P. aeruginosa* complete genomes from GenBank. Quality evaluation of raw data was done with FastQC software (https://github.com/s-andrews/FastQC). Poor quality reads were trimmed with Sickle (version 1.210) and transposase adaptor contaminations were eliminated with Cutadapt (v2.6) [122]. The sequence of the adaptor was found in the following website: https://github.com/golharam/FastQC/blob/master/Configuration/adapter_list.txt. Assembly of raw sequence data was performed with SPAdes (http://cab.spbu.ru/software/spades/) and quality assessment with QUAST (v5.0.2) [123]. Genome annotation was done using Prokka (v1.14.0)[124].

Phylogenetic analysis

Multi locus sequence typing (MLST) was conducted with mlst (v2.17.6) (https://github.com/tseemann/mlst) and PubMLST website (https://pubmlst.org/), developed by Keith Jolley [125]. Pangenome and core gene alignments were created with Roary [126]. The roary core genome alignments were created with MAFFT sequence alignment programme. SNPs were identified with Snippy [127] on raw sequence data and with Roary on the assembled genomes. Maximum likelihood phylogenetic trees were constructed with RaxML applying the GTR (general time reversible) substitution model, bootstrapping 100, 10 parsimony, and with gamma distributed variation [128]. Genome alignment files for RaxML were obtained from Roary using mafft alignment or Snippy-core with DHS01 as reference genome. SNP distances were calculated with Snp-dists (https://github.com/tseemann/snp-dists) on the Roary and Snippy alignments. Additionally, alternative phylogenetic trees were constructed with ParSNP assigning one of the sequences as reference sequence at random [129]. The trees

were visualised in FigTree (http://tree.bio.ed.ac.uk/software/figtree/) and the additional metadata were visualised in the online tool Phandago [130].

Identification of ARGs and GIs

Resistance gene presence was identified with Abricate (v0.9.8) (https://github.com/tseemann/abricate) and searched in the NCBI AMRFinderPlus database [131]. The identified GIs were searched against local databases of the additional ST395 strains and the dataset 3, as obtained from GenBank until April 2020.

Results

De novo assembly

The raw reads of all isolates were examined for adaptor contamination and low-quality sequences with FastQC software. The twelve sequences contaminated with Nextera transposase adaptor sequences were curated using the Cutadapt programme. All reverse sequence reads were of middle to poor quality (> 30 Phred score). So, all pair-end data were trimmed with Sickle using a cut-off quality of 25 and window length of 15 bp. Afterwards, the sequences were assembled using SPAdes. The evaluation of the assemblies was conducted with the Quast.py tool on the contigs.fasta files of the assemblies. All sequences, including PT_F and PAO1 which were downloaded as complete genomic sequences, were *de novo* annotated using Prokka.

The authors incorporated six ST395 genomic sequences and 10 non-ST395 in their research while both bioprojects contained 19 sequence data (excluding PAO1, DHS01, and PT_F). In order to recognise whether these sequences belonged to the *P. aeruginosa* species, their ST type was characterised via the MLST tool mlst and search in the PubMLST website. All additional sequences were categorised as ST395 isolates. Table 3 shows the isolates and their ST.

Pangenome analysis

Every species has a core genome, i.e. genes shared among all members of a species, and accessory genome which refers to "dispensable genes not found in every strain" [132]. When combined, they constitute the pangenome which includes all

gene families detected within this species [132]. Here, two datasets were submitted to pangenome analysis with Roary. Dataset 1 is comprised of the *de novo* assembled genomes of table 3, as well as those of PAO1 and PT_F. PT_F is the genome of a ST395 isolate from Birmingham. Dataset 2 includes DHS01 and the 82 complete genome sequences of *P. aeruginosa* available in GenBank until July 2017, which were also used in the present paper. Roary is a tool for rapidly building large-scale pangenomes and identifying the core and accessory genes [126].

Name in the paper	Included in the (Petitjean et al. 2017) paper	Sequence Type (ST)
DHS01	YES	395
PT_B	YES	395
PT_C	YES	395
PT_D	YES	395
PT_E	YES	395
PT_F	YES	395
PT_G	YES	395
PT_H	NO	395
PT_I	NO	395
PT_J	NO	395
PT_K	NO	395
PT_L	NO	395
ST111	YES	111
ST175a	YES	175
ST175b	YES	175
ST233	YES	233
ST235a	YES	235
ST235b	YES	235
ST348	YES	348
PAO1	YES	549
ST1342	YES	1342
ST1602	YES	1602

Table 3. List of isolates in dataset 1 and their ST.

The core genome of dataset 1 was estimated at 5,005 genes and the pangenome at 11,403 genes. Past research has indicated the core genome size in the range of 5,200 and 5,300 genes[119,120], which is close to the core genome

predicted here. . The pangenome was significantly larger than the pangenome (9,344 genes) predicted by Valot *et al.* (2015). The size difference could be due to *P. aeruginosa* having an open genome [133] which means that the pangenome will expand with every new strain added to the analysis. Considering that the average genome size of ST395 is 7.00 Mbp, with the highest genome of the species being 7.56 Mbp, it is not unexpected to observe a high number of accessory genes. As can be seen in figure 10, all ST395 share a small panel of genes that is generally absent from the other strains. The majority of these genes constitute genes of hypothetical proteins.

Pangenome analysis of the second dataset showed a different picture. The core genome was composed of 2,837 genes and the pangenome of 20,363. The authors calculated the core genome at 1973 genes, which could be a result of the different procedures followed. Here, Roary was used for the task while MuMmer [134] was the programme of choice in the paper. Whereas the large pangenome size was anticipated, judging by the size of the dataset (83 genomes), the core genome was remarkably small. One reason might be the inclusion of the taxonomic outlier strain PA7 which could bias the outcome of the core genome analysis [120]. If we looked at the soft-core genes, those present at 95% of the studied genomes, we would see that there were 2,293 additional genes. The sum of the core and soft-core genes (5,030) is close to the predicted core genome of the species.

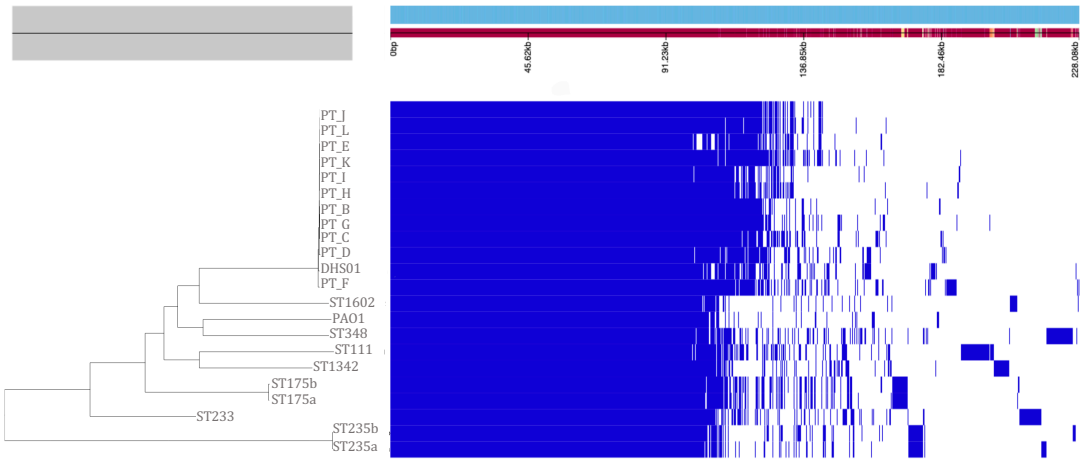

Figure 10. Pangenome of Dataset 1. The pangenome was constructed with Roary and the tree is made with Roary core genome alignment and RaxML. Blue colour indicates existence of a gene in the genome of a strain. The bar on top of the pictures shows the size of the pangenome in kbs if every gene was 20 bp long. The ST395 isolates seems to share a number of genes that are largely missing from the other STs.

Phylogenetic analysis

Following on the pangenome analysis, phylogenetic trees with both datasets 1 and 2 were constructed. In each case, three different procedures were implemented: 1) use of the assembled contigs and ParSNP pipeline to create a fast and less accurate tree, 2) the assembled contigs aligned with Snippy against the reference strain DHS01 and the phylogenetic inference programme RaxML, and 3) the Roary alignment and RaxML. Regarding dataset 2, the fasta files from GenBank were used in place of the contigs files.

ParSNP is a pipeline for whole genome assembly phylogenetic analysis and is designed for intraspecific genome analysis. It aligns all sequences against one reference sequence and infers phylogenetic trees based on the ubiquitously existing regions. One main limitation of ParSNP is that it can work with core-genomes and is not as sensitive as other existing methods. ParSNP functions better in the analysis of high-quality assemblies or when raw read data are not available [129]. Snippy searches for single nucleotide polymorphisms (SNPs) between a haploid reference genome and NGS sequence reads [127]. Snippy will identify both SNPs and insertions/deletions, and can be used to create a core-genome alignment. RaxML is a rapid maximum likelihood-based inference of large evolutionary trees [128]. It takes as input a genome alignment, such that generated by Snippy or Roary, and outputs a phylogenetic tree.

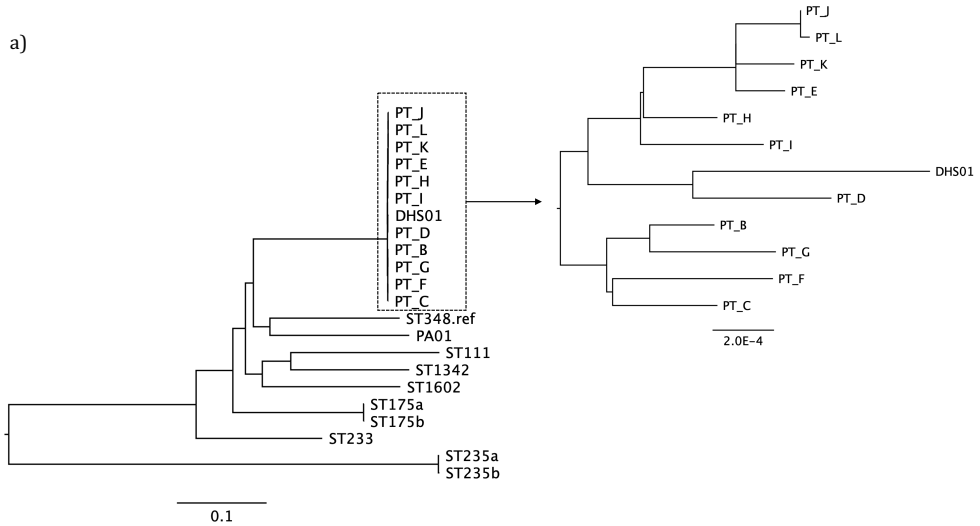

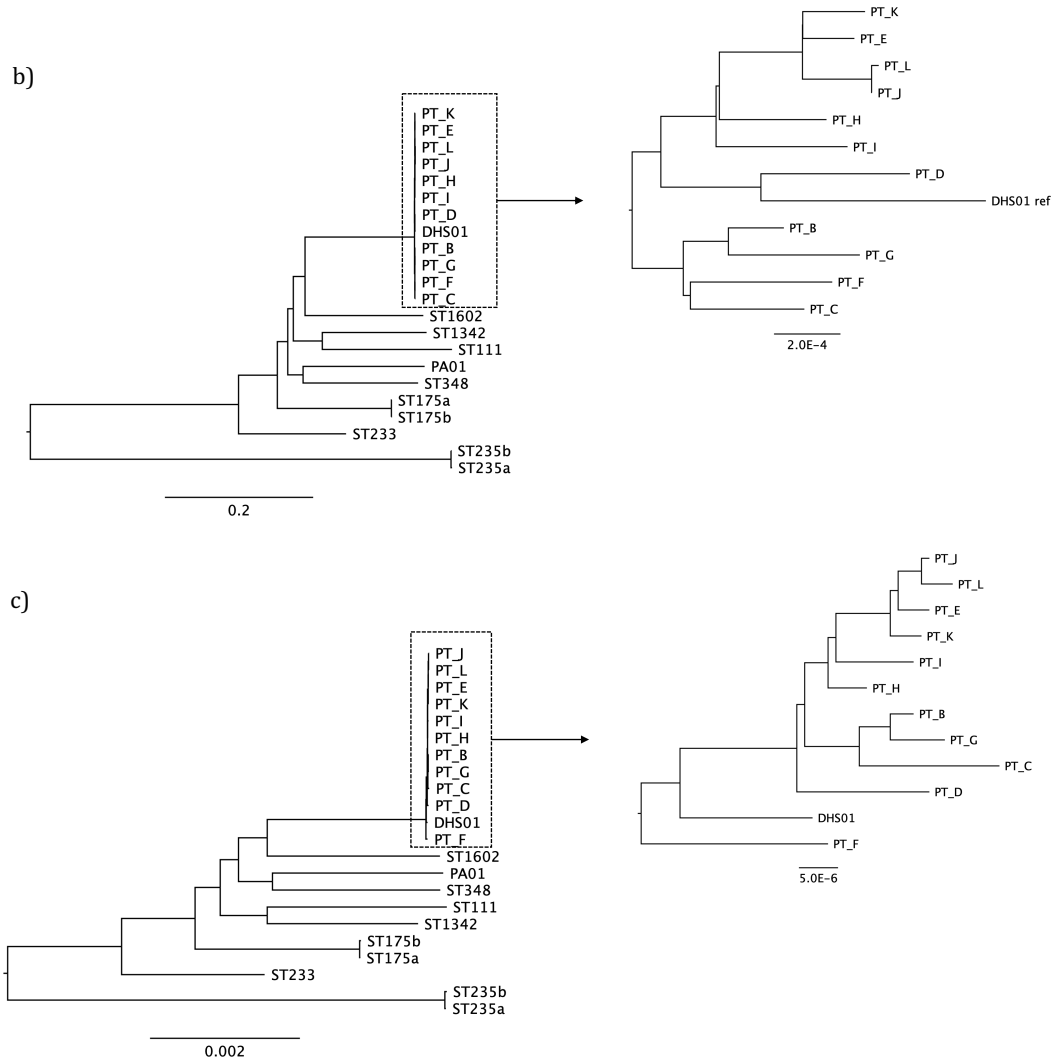

Figure 11. Phylogenetic analysis of Dataset 1. The trees were constructed with three different procedures: a) ParSNP, b) Snippy core genome alignment and RaxML, c) Roary core genome alignment and RaxML. All trees depict similar phylogenetic relationships regardless of the applied procedure. An important difference was the substitution per site rate. The tree made of the Roary alignment exhibited the smallest rate while ParSNP had the highest. This variance could be attributed to the different way the programmes calculate SNPs. For information on parametres and algorithms used, see "Materials and Methods" section.

The phylogenetic trees of dataset 1 produced almost identical results (fig. 11), differing only in the position of two clades. The tree constructed with ParSNP positioned the clade of ST1602 closer to that of the ST395 isolates. In contrast, Snippy tree placed the PAO1 and ST348 closer to the ST395. The major variation among the trees was the scale bar of substitution per site. The highest rate was predicted by the Snippy alignment (0.2) and the lowest was that of Roary (0.002). The results could arise from the fact that Roary takes into account mutations

inside ORFs while Snippy and ParSNP include all genomic areas in their analysis. A comparison of the SNP distances between Snippy and Roary alignments demonstrates significant differences. In all cases, Snippy calculated more SNPs among different ST isolates than Roary. The opposite was true for SNPs within the ST395 group. A plausible explanation could be that Snippy utilises assembled sequence files which contain all sequence data reads contributed in the assembly. This way, Snippy can deduct the likelihood of a SNP to be valid and filter out the low-quality SNPs. On the other hand, Roary uses pre-annotated GFF3 files which have information on every feature that can be applied on a nucleic acid or protein sequence but do not inform on the quality of each base or residue.

The publication tree was made by aligning the sequences with MuMmer [134] and inferring phylogeny with PhyML [135]. Overall, the trees generated by ParSNP and Roary alignment/RaxML were similar to that of the publication (fig. 12). Small variations occurred, mainly on inner branches positions. However, the genomes cluster in the same two sets, those more related to PA14 (UCBPP-PA14 in fig. 12) and those related to PAO1. In the latter category belongs DHS01 which is also clustered with the LESB58 and LES431 isolates. They belong to the highly virulent epidemic strain LES (Liverpool Epidemic Strain) [136]. Strikingly, the tree obtained by Snippy core alignment and RaxML differed to the previous three. Even though the two clusters were formed, the PA14 cluster is placed as a subclade of the PAO1 cluster. Since RaxML was used for constructing the phylogenetic tree from the Roary core alignment, the observed dissimilarity might be attributed to Snippy alignment. For the Snippy alignment, all sequences were compared to the reference genome of DHS01. Equally to the dataset 1, the substitution per site scales are not similar. The greatest scale is predicted by Snippy and RaxML, and the minimum by Roary core alignment and RaxML.

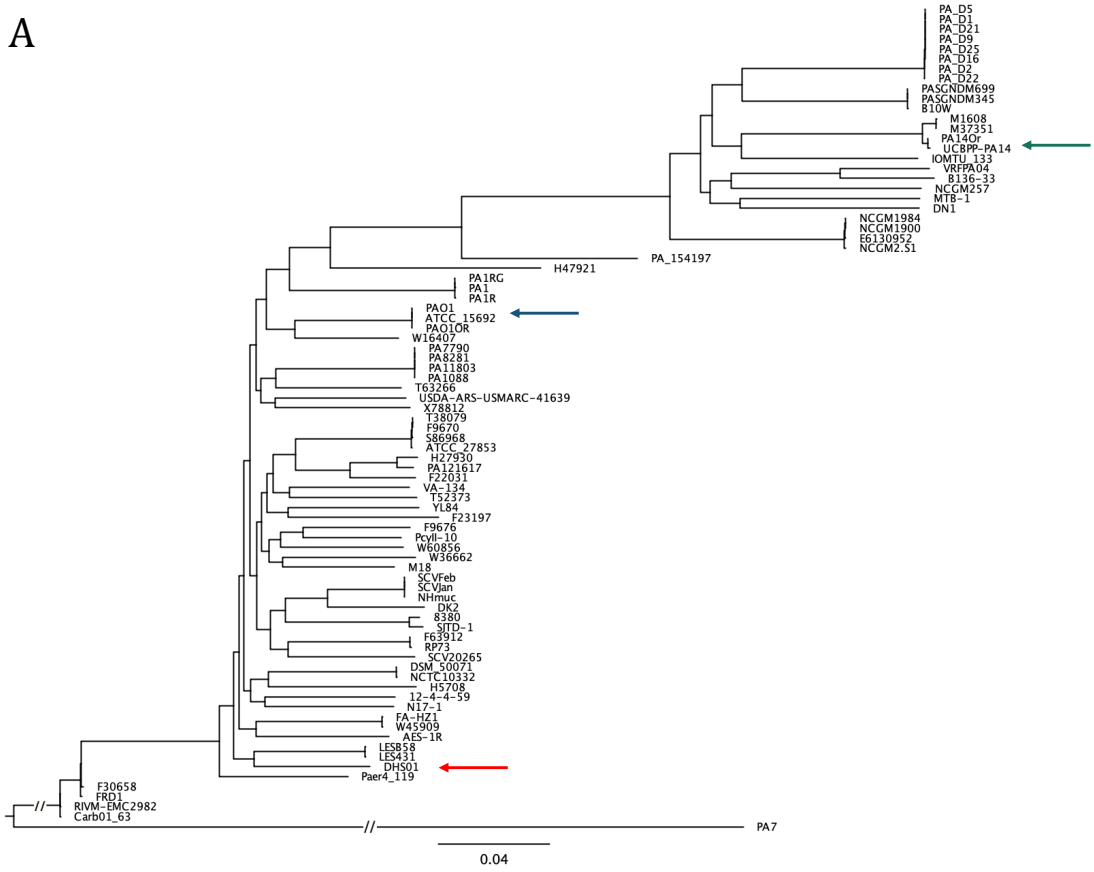
A
PA_D5
PA_D1
PA_D21
PA_D9
PA_D25
PA_D16
PA_D2
PA_D22
PASGNDM699
PASGNDM345
B10W
M1608
M37351
PA14Or
UCBPP-PA14
IOMTU_133
VRFPA04
B136-33
NCGM257
MTB-1
DN1
NCGM1984
NCGM1900
E6130952
NCGM2.S1
H47921
PA_154197
PA1RG
PA1
PA1R
PAO1
ATCC_15692
PAO1OR
W16407
PA7790
PA8281
PA11803
PA1088
T63266
USDA-ARS-USMARC-41639
X78812
T38079
F9670
S86968
ATCC_27853
H27930
PA121617
F22031
VA-134
T52373
YL84
F23197
F9676
Pcyll-10
W60856
W36662
M18
SCVFeb
SCVJan
NHmuc
DK2
8380
SJTD-1
F63912
RP73
SCV20265
DSM_50071
NCTC10332
H5708
12-4-4-59
N17-1
FA-HZ1
W45909
AES-1R
LES858
LES431
DHS01
Paer4_119
F30658
FRD1
RIVM-EMC2982
Carb01_63
PA7
0.04

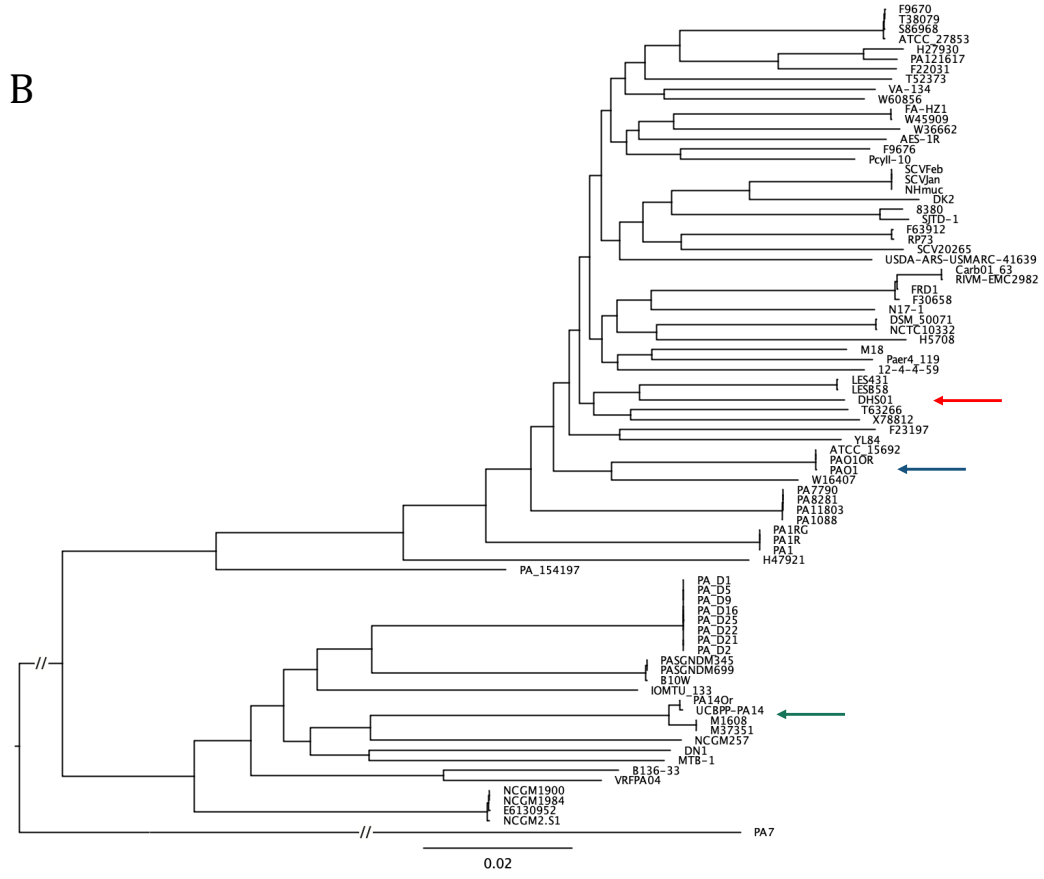
B
F9670
T38079
S86968
ATCC_27853
H27930
PA121617
F22031
T52373
VA-134
W60856
FA-HZ1
W45909
W36662
AES-1R
F9676
Pcyll-10
SCVFeb
SCVJan
NHmuc
DK2
8380
SJTD-1
F63912
RP73
SCV20265
USDA-ARS-USMARC-41639
Carb01_63
RIVM-EMC2982
FRD1
F30658
N17-1
DSM_50071
NCTC10332
H5708
M18
Paer4_119
12-4-4-59
LES431
LES858
DHS01
T63266
X78812
F23197
YL84
ATCC_15692
PAO1OR
PAO1
W16407
PA7790
PA8281
PA11803
PA1088
PA1RG
PA1R
PA1
H47921
PA_154197
PA_D1
PA_D5
PA_D9
PA_D16
PA_D25
PA_D22
PA_D21
PA_D2
PASGNDM345
PASGNDM699
B10W
IOMTU_133
PA14Or
UCBPP-PA14
M1608
M37351
NCGM257
DN1
MTB-1
B136-33
VRFPA04
NCGM1900
NCGM1984
E6130952
NCGM2.S1
PA7
0.02

C

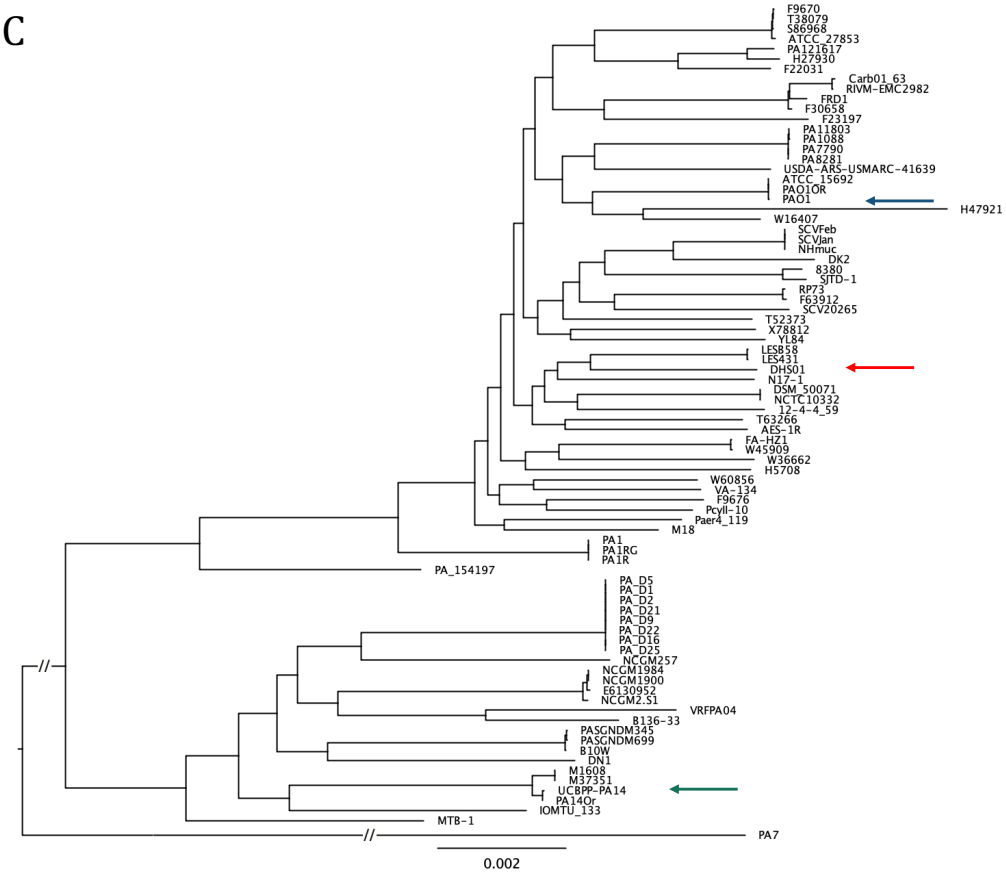
F9670
T38079
S86968
ATCC_27853
PA121617
H27930
F22031
Carb01_63
RIVM-EMC2982
FRD1
F30658
F23197
PA11803
PA1088
PA7790
PA8281
USDA-ARS-USMARC-41639
ATCC_15692
PAO1OR
PAO1
H47921
W16407
SCVFeb
SCVJan
NHmuc
DK2
8380
SJTD-1
RP73
F63912
SCV20265
T52373
X78812
YL84
LES858
LES431
DHS01
N17-1
DSM_50071
NCTC10332
12-4-4_59
T63266
AES-1R
FA-HZ1
W45909
W36662
H5708
W60856
VA-134
F9676
Pcyll-10
Paer4_119
M18
PA1
PA1RG
PA1R
PA_154197
PA_D5
PA_D1
PA_D2
PA_D21
PA_D9
PA_D22
PA_D16
PA_D25
NCGM257
NCGM1984
NCGM1900
E6130952
NCGM2.S1
VRFPA04
B136-33
PASGNDM345
PASGNDM699
B10W
DN1
M1608
M37351
UCBPP-PA14
PA14Or
IOMTU_133
MTB-1
PA7
0.002

D

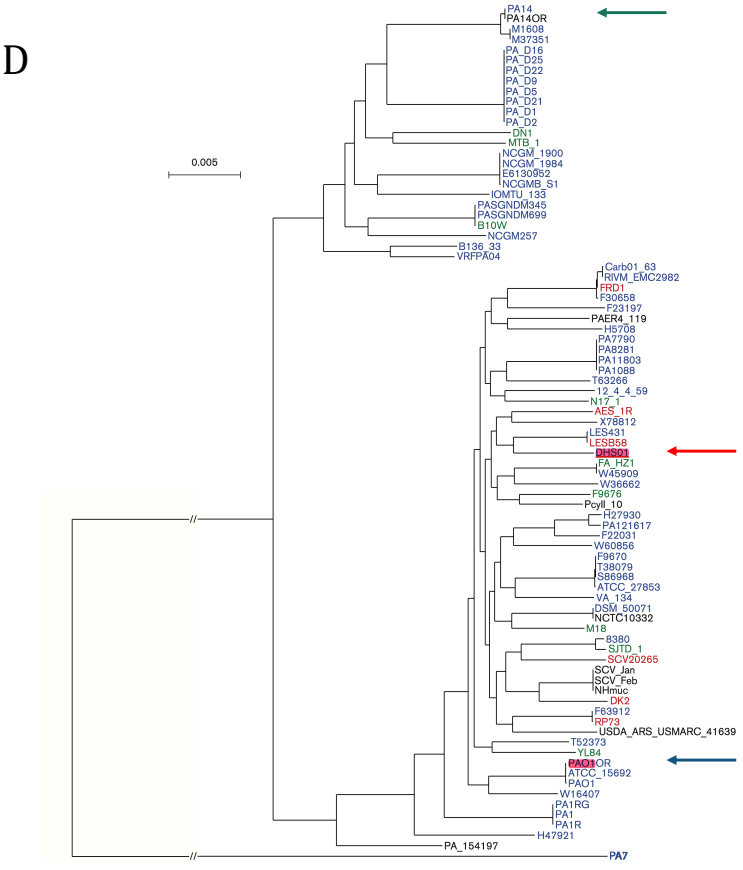
PA14
PA14OR
M1608
M37351
PA_D16
PA_D25
PA_D22
PA_D9
PA_D5
PA_D21
PA_D1
PA_D2
DN1
MTB_1
NCGM_1900
NCGM_1984
E6130952
NCGMB_S1
IOMTU_133
PASGNDM345
PASGNDM699
B10W
NCGM257
B136_33
VRFPA04
0.005
Carb01_63
RIVM_EMC2982
FRD1
F30658
F23197
PAER4_119
H5708
PA7790
PA8281
PA11803
PA1088
T63266
12_4_4_59
N17_1
AES_1R
X78812
LES431
LESB58
DHS01
FA_HZ1
W45909
W36662
F9676
Pcyll_10
H27930
PA121617
F22031
W60856
F9670
T38079
S86968
ATCC_27853
VA_134
DSM_50071
NCTC10332
M18
8380
SJTD_1
SCV20265
SCV_Jan
SCV_Feb
NHmuc
DK2
F63912
RP73
USDA_ARS_USMARC_41639
T52373
YL84
PAO1OR
ATCC_15692
PAO1
W16407
PA1RG
PA1
PA1R
H47921
PA_154197
PA7

Figure 12. Phylogenetic analysis of Dataset 2. The phylogenetic trees were obtained following three different procedures: A) Core genome alignment by Snippy core and RaxML programme for tree inference, B) ParSNP pipeline, C) Core genome alignment using Roary and RaxML for producing the phylogenetic tree, D) The tree from Petitjean *et al.* (2017) paper. Overall, the trees constructed with ParSNP and Roary core alignment (B and C respectively) are similar to the one in the publication. However, the tree produced with Snippy core alignment places the PA14 cluster as a subgroup of PAO1 cluster demonstrating the dependence of the outcome on the choice of computational programmes. Arrows: Red, DHS01; Green, PA14; Blue, PAO1. For information on parametres and algorithms used, see "Materials and Methods" section.

ARG detection

Search for AMR genes (table 4, fig. 13) revealed 30 ARGs present in at least one of the isolates. The majority of them (13 out of 30) encoded for β-lactam resistance followed by aminoglycoside resistance genes. Almost all genes for aminoglycoside and β-lactam resistance were found outside of the ST395 and PAO1 strains (fig. 13) with the exception of *aph(3')-llb* gene. Additionally, the chloramphenicol resistance *catB7* and fosfomycin resistance *fosA* were found in all strains. The OXA-50 family (oxacillin-hydrolysing class D beta-lactamase *blaOXA-488*) was only encoded in the ST395 and ST235 strains. Presence of *crpP blaPDC-374* was not detected in PAO1, ST233, and the two ST235 and ST111 and ST1342, respectively.

Antibiotic classes	Identified ARGs
B-lactam	*blaCARB-2, blaIMP-19, blaIMP-29, blaOXA-19, blaOXA-28, blaOXA-395, blaOXA-396, blaOXA-486, blaOXA-488, blaOXA-494, blaOXA-50, blaPDC-374, blaPDC-55*
Aminoglycoside	*aac(6')-Ib, aac(6')-Ib4, aadA11, aadA13, aadA2, aadA6, ant(2'')-Ia, aph(3'')-Ib, aph(3')-IIb, aph(6)-Id*
Chloramphenicol	*catB7, cmlB1, floR2*
Trimethoprim	*dfrB1*
Quinolone	*crpP*
Sulphonamide	*sul1*
Fosfomycin	*fosA*

Table 4. Identified ARGS and antibiotic class they belong to. Red: found in all strains, Blue: almost all strains

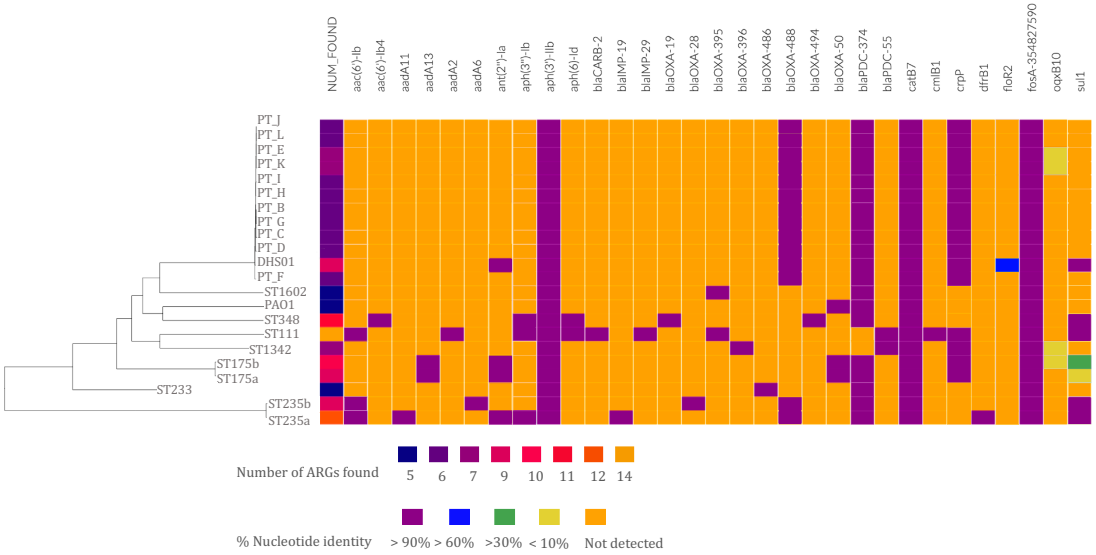

Figure 13. Presence of ARGs in strains of Dataset 1. The construction of the phylogenetic tree was done using Roary core alignment and RaxML. The identification of ARGs was conducted with Abricate. Orange colour indicates absence of the specified ARG whereas purple indicates over 90% nucleotide identity to the ARG sequence in the database used in the search. Here the NCBI AMRFinderPlus database was implemented in the search. Only three ARGs were present in all strains tested while none of them was found exclusively in ST395 strains.

GI detection

The authors sought to identify particular genomic features of the ST395 that render it a high-risk clone. The genome of DHS01 harbours 48 GIs according to the publication. Eight of them (GI-1 to GI-8) were detected only in strains of the ST395. Half of these GIs were ubiquitously found in all strains except for GI-7 that was also present in 2 ST235 strains, according to the publication. The region of GI-7 is comprised of an array of six genes for copper transporters, including the genes *copA* and *copB*. It was hypothesised that resistance to copper was a crucial element for the dissemination of ST395 through the water network of the Hospital of Birmingham [117]. All strains were experimentally tested for copper resistance resulting in all of them surviving copper-containing media after 48 h of incubation. For this reason, it was deemed necessary to search the existence of GI-7 in the other five ST395 isolates. Local Blast search of the GIs against the extra five ST395 isolates (PT_H - PT_L) revealed that all strains carried GI_4 to GI-7 while most of them lack GI-1 and GI-3.

The authors searched for the presence of these GIs in the 82 complete sequences of *P. aeruginosa* available until July 2017. By April 2020, 221 complete *P. aeruginosa* genomes had been deposited in GenBank. So, it was also investigated whether any of these GIs would be retrieved from the more expanded collection of complete genomes. Blast search of the eight GIs showed that they were specifically found in ST395 strains only. Surprisingly, the exception to the rule was GI-7. It was also present, completely intact, in four ST235, one ST111, and all five ST309 genomes included in the search (table 5). All of them were clinical isolates with apart from one environmental ST235. The other GIs were partially present or completely omitted in other STs. Although ST395 may rely on copper resistance for its dissemination and persistence in nosocomial settings, the wider prevalence of an intact G7 might point to an evolutionary advantage for the host.

Accession number	Strain	MLST	Isolate	Country
NZ_CP026680.1	F5677	111	clinical	New York
NZ_CP008862.2	M1608	253	clinical	New York
NZ_CP008863.1	M3751	253	clinical	New York
NZ_CP019338.1	L10	253	environmental	China
NZ_CP033685.1	H26023	253	clinical	Switzerland
NZ_CP021774.1	Pa124	309	clinical	Mexico
NZ_CP022000.1	Pa127	309	clinical	Mexico
NZ_LR130533.1	paerg0090	309	clinical	Switzerland
NZ_LR130534.1	paerg005	309	clinical	Switzerland
NZ_LR739069.1	PcyII-40	309	clinical	France
NZ_CP013993.1	DHS01	395	clinical	France
NZ_CP023255.1	CCUG_70744	395	clinical	Sweden
NZ_CP029090.1	AR442	395	clinical	USA
NZ_CP046060.1	1811-18R001	395	clinical	China
NZ_CP046061.1	1811-13R031	395	clinical	China

Table 5. Strains harbouring GI-7. Search in Pseudomonas.com and PubMed for source identification.

Discussion

The implementation of NGS technologies in the fight against AMR has aided in the surveillance and infection control of MDR pathogens. More and more computational pipelines become largely available, facilitating the execution of

bioinformatic research by non-specialist microbiologists. However, various programmes could produce different results rendering the interpretation and reproducibility of the research dependent on the tools employed.

P. aeruginosa is an MDR pathogen causing high rates of morbidity and mortality to CF patients. Despite its non-clonal population structure, a few clones have infiltrated nosocomial environments across the world. Among these is ST395, a highly virulent clone which has been identified in a number of outbreaks [117,136,137]. Petitjean *et al*. (2017) investigated the genomic features which have permitted the spread and persistence of ST395. The genome of DHS01, an isolate from an outbreak in a French hospital, as well as those of a panel of ST395 and non-ST395 isolates were sequenced. The comparison of the sequenced genomes aided in the characterisation of ST395 specific features. The large genome of DHS01 possessed five integrative conjugative elements, a plethora of ARGs, mutations in ARG regulators conferring resistance, fewer virulence factor than the reference strain PAO1, and a degenerated CRISPR-Cas system. In addition, 48 GIs were spotted, out of which eight were ST395 specific. The GI-7 encoded for six copper transporters which was hypothesised to be the reason of ST395 dissemination through hospital water networks.

In the present bioinformatics project, the raw sequence data of the [112] paper were *de novo* assembled, annotated, and the pangenome was defined. Additionally, they ARGs were defined and phylogenetic trees were constructed with three different approaches. Moreover, phylogenetic trees were constructed and the pangenome was defined using the sequences of 82 complete *P. aeruginosa* genomes and compared to those in the paper. Lastly, the eight GIs of ST395 were searched against an additional set of five ST395 genomes present in the raw data of the paper, as well as all the available complete *P. aeruginosa* genomes in GenBank.

The core genome of the *de novo* assembled genomes (dataset 1) was calculated at 5,005 genes, close to the pangenome extrapolated by previous research, and the pangenome at 11,403 genes. In contrast, the core genome of dataset 2, as calculated by Roary, included 864 genes more than that of the prediction of the paper examined here. The assessment of different core genomes illustrates that the choice of programme and the algorithms designed for it

influences the outcome of the research. Nevertheless, the fact that PA7 strain was included in both cases significantly reduced the estimated core genome. Ozer *et al.* (2014) discovered that PA7 lacked 476 kbp DNA which was present in the other 11 *P. aeruginosa* strains they studied. It encoded for several typical features of the species, such as the exotoxin A gene. Therefore, applying more flexible conditions in the search of core genome could facilitate a better perception of the conservation of a gene within a species.

The phylogenetic trees generated with dataset 1 were highly similar. Even though one of them was constructed with the ParSNP pipeline, which is faster but less accurate than other existing programmes, the employment of ParSNP here produced similar results to that of RaxML. A conclusion might be that depending on the task and biological question to be answered, a less accurate programme could be equally suitable for the task as more sensitive but time-consuming programmes. However, not all trees from dataset 2 matched the published tree. The Snippy/RaxML tree depicted an alternative evolutionary picture. In this case, generating more than one tree by a variety of procedures could increase the confidence to the analysis. If only the tree from Snippy/RaxML analysis was available, then the interpretation and subsequent procedures might have been distorted.

The presence of antibiotic resistance genes was performed using Abricate. Overall, 30 ARGs were identified in the genomes of dataset 1, most of them related to β-lactam and aminoglycoside resistance. According to the publication, DHS01 exhibits MDR phenotype, with resistance to gentamycin, tobramycin, ciprofloxacin, and β-lactam compounds but it was susceptible to cefepime, ceftazidime, imipenem, and amikacin. The resistance profile of this isolate was attributed to mutations in regulators such as *mexZ* and *ampR*, as well as to the 2' Aminoglycoside nucleotidyl-transferase (*ant(2'')-Ia*) expression and the overproduction of AmpC cephalosporinase. The gene *ampC* was not retrieved in the present research. It suggests that irrespective of the results of the ARG search, the isolates may be resistant to more antibiotic classes than those identified, and the source of resistance may be mutations in non-ARGs. Since the other ST395 isolates bore 108-168 SNPs in relation to DHS01, it could be hypothesised that

they are also resistant to the same antibiotics despite the small number of harboured ARGs.

Lastly, ST395 was shown in the publication to possess eight GIs, with GI-7 conferring resistance to copper. The present research revealed that GI-7 exhibited wider dissemination among *P. aeruginosa* isolates than any other ST395-specific GI. It was present in genomes of ST111, ST235, and all genomes of ST309. ST111, ST235, and ST395 have been previously characterised as high-risk clones [115]. On the other hand, ST309 was not associated with global manifestation in hospital outbreaks. Recently, ST309 isolates were linked to extensive drug-resistant (XDR) and MDR phenotypes in children bacteraemia in Mexico [138]. Additionally, it was present in an outbreak in a Greek hospital[139] and one in the United States [140]. It is also evident from table 5 that the ST309 carrying GI-7 were isolated in three different countries (Mexico, Switzerland, France). These are indications of broader spread of ST309, suggesting that it may also be a high-risk clone.

Generally, copper resistance has been more prevalent in hospital dwelling *P. aeruginosa* strains than their environmental counterparts [141]. However, the resistance to copper was not associated to previously characterised processes implicating *copA* and *copB,* which implies other underlying networks might be responsible for the phenotype [141]. It has been demonstrated that pure copper surfaces (99% copper) have a greater bactericidal activity against MDR pathogens, including *P. aeruginosa*, than surfaces consisted of 63% copper [142]. The fact that GI-7 harbours six copper transporters might increase the already intrinsic resistance of *P. aeruginosa* strains allowing for longer survival in the copper plumbing systems of hospitals.

Chapter 4: General Discussion - Perspectives for the next three years

In the previous chapter, the genetic determinants of *P. aeruginosa* highly virulent clone ST395 were discussed. WHO has included *P. aeruginosa* in the list of pathogens of critical priority, for which antimicrobial R&D should be prioritised [143]. *P. aeruginosa* is intrinsically resistant to many of the current antibiotics and produces a variety of virulence factors facilitating the establishment and continuation of infections [113,144–146]. These factors are host-specific and under the control of multiple communication regulatory networks, named quorum sensing (QS) systems [147]. Targeting the QS systems of *P. aeruginosa* has attracted significant attention due to its controlling biofilm formation and synthesis of virulent factors [95]. Therefore, virulence can be attenuated without the promotion of selective pressure to the same levels as these of antibiotics [148].

QS systems are based on the synthesis and diffusion of a QS signal molecule, called autoinducer. When it reaches a critical extracellular concentration, reflecting the population density, it re-enters the cells, binds its respective system receptor, and alters expression of target genes. Additionally, the regulator-autoinducer pair often upregulates its cognate synthase production creating a positive feedback loop.

At least three self-regulating interdependent QS systems have been described in *P. aeruginosa*. Two of them, the LuxRI-type LasRI (*las*) and RhlRI (*rhl)* systems, utilise *N*-acyl-homoserine lactone as their effector molecules. The LasI synthase produces the ligand *N*-(3-oxododecanoyl)-*L*-homoserine lactone (3-oxo-C_{12}-HSL) of the receptor LasR. Similarly, RhlI synthase produces *N*-butanoyl-*L*-homoserine lactone (C_4-HSL) which binds to the receptor RhlR. The *rhl* system is also induced by the *las* system. These two systems direct the expression of various virulence genes, such as those required for the synthesis of exotoxin A, hydrogen cyanide, and pyocyanin (PYO), in addition to the genes of the third QS system, *pqs.* The *pqs* system is dependent on 2-alkyl-4(1*H*)-quinolone (AQ) molecules and controls the production of many virulence factors including elastase, lectin A, PYO, biofilm formation, and swarming motility, thus contributing to acute and chronic infection establishment [149,150].

Until now, more than 50 AQ molecules have been found to be produced by *P. aeruginosa* [151]. The 2-heptyl-4-hydroxyquinoline (HHQ) and 2-heptyl-3-hydroxy-4-quinolone, also referred to as the *Pseudomonas* quinolone signal (PQS), are potent QS signals [151]. The first step of QS biosynthesis is the conversion of chorismic acid to anthranilate by PhnAB, in addition to the contributions of TrpEG and the kynurenine pathway in anthranilate accumulation [152,153]. The anthranilate coenzyme A ligase PqsA combines anthranilate and CoA to anthraniloyl-CoA, and PqsD condenses it with malonyl-CoA to 2-aminobenzoylacetyl-CoA (2-ABA-CoA) [154,155]. Afterwards, the thioesterase PqsE converts it into 2-aminobenzoylacetate (2-ABA) and subsequently HHQ is formed via the activity of PqsBC complex [156,157]. From there, HHQ either remains as it is or is converted to PQS by the monooxygenase PqsH under aerobic conditions, or to 2-heptyl-4-hydroxyquinoline *N*-oxide (HQNO) by PqsL and PqsBC [151,158].

The genetic circuit of the *pqs* system is comprised of two biosynthetic operons, *pqsABCDE* (locus tag PA0996-PA1000, as annotated for the reference strain PAO1) which lies next to the second operon, the phenazine synthesis *phnA-B* (locus tag PA1001-1002) (fig. 14). Adjacent to the latter and divergently transcribed, is the gene of their transcriptional regulator PqsR, also known as MvfR (locus tag PA1003). The *pqsL* (PA4190) and *pqsH* (PA2587) genes reside elsewhere on the chromosome.

Mutations in the *pqsABC* and *D* genes hinder the production of AQs whereas deletion of *pqsH* or *pqsL* leads to the accumulation of HHQ and HQNO, or HHQ and PQS, respectively. PqsE is redundant in AQ biosynthesis, possibly because TesB thioesterase can substitute for PqsE absence [157]. However, PqsE seems to be the effector protein of the *pqs system* since it controls PYO biosynthetic genes, biofilm formation and swarming motility through an unidentified mechanism [149,150]. Also, PqsE restores virulence in nematode, plant and mouse infection models in a *pqsA* mutant strain [149,150].

PYO is a redox-active phenazine pigment, important in *P. aeruginosa* acute and chronic lung infections [159]. The regulation of PYO is controlled by the three QS systems, with RhlR and PqsE being indispensable [160]. PYO biosynthesis begins with the conversion of chorismic acid to phenazine-1-carboxylic acid (PCA-1) by

the action of the enzymes of the two almost identical *phzABCDEFG* operons, *phz1* and *phz2* [161] (fig. 15). Then, PhzM and PhzS convert PCA-1 to PYO [161].

Even though HHQ might solely induce the expression of *pqsA-E* operon via PqsR, PQS possesses a broader spectrum of roles than inducing its own biosynthesis [149]. PQS enhances OM vesicle biogenesis, chelates iron on the cell membrane thereby activating iron-starvation response, induces cytotoxicity through oxidative stress and slower growth rate, and induces host immunomodulatory activities (reviewed in [114]). Therefore, PQS, and by extension the *pqs* system, facilitates survival of *P. aeruginosa* in diverse environmental conditions and provides fitness advantage in mixed microbial populations.

The *pqs system* is activated in late stationery phase [162]. Mainly, the *pqsABCDE* operon and the *phnAB* operon are regulated by the LysR-type regulator PqsR [163–165]. PqsR binds either PQS or HHQ, and the ligand-regulator complex binds the LysR-binding box (PqsR-binding box) upstream of *pqsA* inducing expression of the operon [163,166]. Factors positively controlling PqsR are the RsaL protein which increases *pqsR* transcription [167], and the regulatory RNA PhrS [168]. Characterised repressors of *pqsR* are the histone-like nucleoid structuring protein, H-NS, MvaT, and MvaU; the LysR transcriptional regulator CysB [169]; and the YebC protein PmpR [170].

Additionally, the *pqs* operon is controlled by other factors. Overexpression of *pqsE* completely represses *pqsA-E* expression in a RhlR-dependent way [150,171]. But in absence of RhlR, PqsE acts as an inducer of *pqs* operon in both PA14 and PA01 [169,171], finely tuning the levels of both PQS and PqsE. The *las* system positively regulates PQS production by inducing transcription of *pqsR* and *pqsH* during mid-exponential phase, and upon entering stationary phase, *pqsR* becomes LasR-independent [166,172,173]. The *rhl* system counteracts the effect of LasR as RhlR downregulates *pqsR* transcription [174]. RhlR was shown to bind directly at the *pqsA* promoter (P_{pqsA}) repressing transcription [175].

Several studies have revealed the significance of small non-coding RNAs (sRNAs) in the regulation of QS systems Djapgne et al. 2018; [168,176–179]. The sRNA PhrD positively regulates RhlR under phosphate-limited conditions [180] and PhrS induces expression of PqsR in response to oxygen depletion [168]. PrrF1 and PrrF2 redundant sRNAs respond to iron starvation by inhibiting expression of non-

essential iron-containing enzymes and increasing PQS synthesis [177]. The catabolite repressor control Crc binds to *phzM* mRNA inhibiting its translation and thereby PYO production [181]. In the presence of non-preferred carbon sources, such as mannitol, CrcZ sRNA sequesters Crc permitting the expression of *phzM* [181]. The CsrA family proteins RsmA/RsmN regulate the transition from acute to chronic infection in response to the two-component system GacA/S [182]. At least four sRNAs, RsmW, RsmV, RsmY, and RsmZ have been found to date binding to and sequestering RsmA/RsmN away from their mRNA targets [182–184].

The biology of sRNAs has been thoroughly reviewed in the past decade [62,185–187]. They are typically 50-500 bp long and they serve a regulatory role at the post-transcriptional level. The majority of sRNAs act through extensive or limited complementarity with their mRNA target, modulating its stability or translation. A minority of them interacts with RNA-binding proteins and sequesters the proteins away from their target. Most of the best characterised sRNAs inhibit mRNA translation by (RBS) of the target mRNA, preventing it from interacting with the ribosome, eventually leading it to decay [185]. RNA degradation in this mechanism mostly occurs through RNases E or III. Other sRNA mechanisms include binding in the coding sequence or the 3' untranslated transcribed region (UTR) of the mRNA. Positive regulatory sRNAs act through: melting mRNA secondary structures which would occlude translation, translation coupling, mRNA structure stabilization, and transcription antitermination [168,188,189]. RNA-binding proteins facilitate and stabilise the interaction between sRNA-mRNA in many occasions. The main RNA-chaperone is the Hfq protein although some sRNAs act Hfq-independently [185,190,191]. There are two main categories of sRNAs: *trans*-acting sRNAs which reside in intergenic regions and their target is distally localised, and the *cis-acting* sRNAs found in the antisense strand of genes (asRNAs). However, sRNAs can be transcribed from within a coding region or formed by processing a mRNA [185].

At least three transcriptional initiation start sites (TSS) have been found at the *pqsA-E* operon region. TSS1 is at -71 bp upstream of *pqsA* [164] and 45 bp downstream of the PqsR-binding box (fig. 14B,C). The second and third TSSs were identified by RNA-seq and verified by 5' RACE PCR [192]. TSS2 is located at -339 from *pqsA* start codon (fig. 14B, C) whereas TSS3 was found 30 bp upstream of *pqsB*.

Upstream of TSS2, lies the LasR/RhlR box, at -381 bp position relative to *pqsA* translational initiation site [192] (fig. 14B,C). Brouwer *et al.* (2014) revealed that RhlR binds to the LasR/RhlR-box and represses *pqsA*[175]. The proposed mechanism was that RhlR induces transcription initiation from TSS2 producing a longer 5' UTR(plong). The plong masks the RBS (9 bp upstream of *pqsA*) of *pqsA* via formation of secondary structures, thus disrupting *pqsA* expression at the post-transcriptional level [175].

On the other hand, previously published RNA-seq data could indicate another mechanism [193]. Wurtzel *et al.* (2012) collected RNA-seq data from PA14 growing at 28 ^{o}C and 37^{o}C and searched for potential sRNA candidates. They discovered a 249 bp sRNA, named Lrs1, located in the intergenic region between the LasR/RhlR box and TSS1 of *pqs* operon (fig. 14). According to their findings, transcription of Lrs1 is dependent on LasR activation, it directly interacts with the RNA chaperone Hfq, and Lrs1 transcripts were abolished in an *hfq* mutant. Deletion of *lrs1* completely inhibited PYO production but had no effect on pyoverdine levels. RNA-seq data from a *Δlrs1* strain showed doubled expression of the anthranilate dioxygenase operon (*antABC*) and a four-fold increase of PrrF1 and PrrF2 sRNAs. The authors speculated that the increase of *antABC* redirected the anthranilate precursor towards the *antABC* pathway, away from PYO production, hence the lack of green colour in a *Δlrs1* culture. Additionally, another study showed the expression of a sRNA from the same region, starting from TSS2 and ending after 175 bp [194]. They predicted an increase in expression of 50 times between exponential and early stationary phase.

Previous transcriptomic analysis of *P. aeruginosa* PAO1 agrees with [193]. The region between LasR/RhlR box and PqsR box seemed to be independently transcribed. Transcriptomic data from stationary phase cultures showed an approximate six-fold increase of transcription of this short area compared to mid-exponential phase. The existence of the sRNA Lrs1 in PAO1 was verified and it will be referred to as PqsX hereafter. Considering that PqsX resides upstream of *pqsA,* it was hypothesised that it might be implicated in the regulation of *pqs.* Previously P_{pqsA} expression levels were measured in the presence of overexpressed *pqsX* [195]. Two regions were overexpressed: a 258 bp region, spanning from the TSS2 to PqsR-box, cloned in the pME6032 expression vector (PqsX-T1), as well as a 337

bp region from TSS2 to the *pqsA* start codon (PqsX-T2) [195]. (fig. 14). The two constructs were then introduced in a *pqsA::lux* expressing PAO1 strain and bioluminescence levels were measured. Both PqsX-T1 and PqsX-T2 were capable of reducing transcriptional levels of *pqsA* by half and translational levels almost 60 times. Thus, the upstream region could exert negative post-transcriptional regulation on P_{pqsA} *in trans*, challenging the proposed model by Brouwer *et al* (2014).

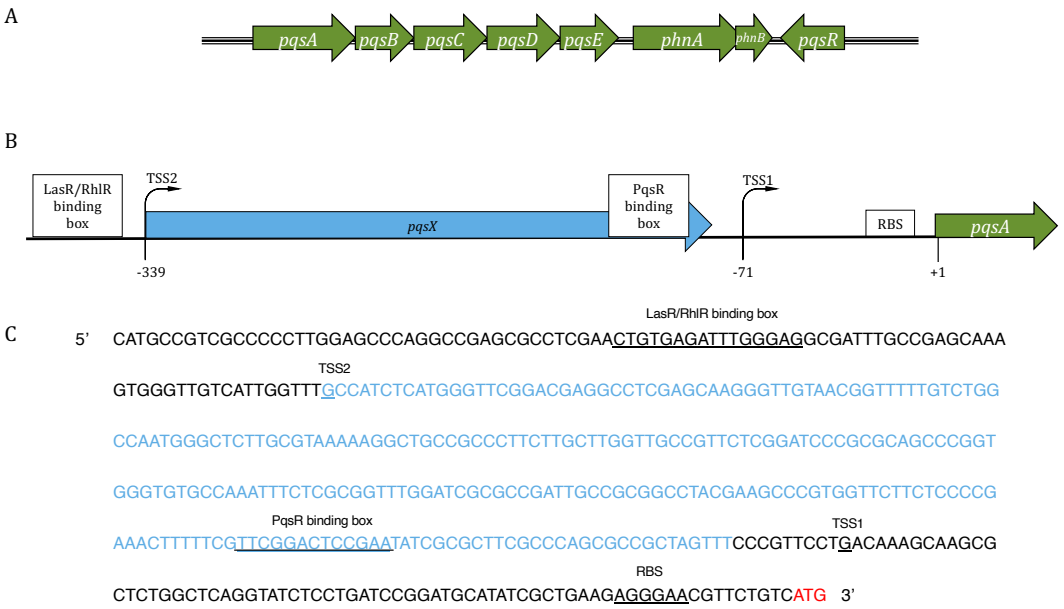

Figure 14. Genetic region of *pqsABCDE* operon in PAO1. 1) Schematic representation of the *pqs* genomic area. Downstream of *pqsABCDE* operon lies the *phnAB* operon which supplies the PqsA with its substrate, anthranilic acid. The *pqsR* gene is located adjacent to *phnAB* and is transcribed in the opposite way. B) Genetic organisation of the region upstream of *pqsA*. The 249 bp *pqsX* (*lrs1* in Wurtzel *et al.* (2012) paper) is located between TSS2 and TSS1, with the 3' end overlapping the PqsR binding box. LasR/RhlR binding box is centred 43 bp upstream of *pqsX*. C) Nucleotide sequence of *pqsA* upstream area. The *pqsX* sequence is coloured in blue. TSS: transcription start site, RBS: ribosome binding site.

Further investigation demonstrated that upon induction of PqsX-T2 in a *ΔpqsA* mutant, PYO production was restored. This indicated another role for PqsX on positively regulating *pqsE* mRNA levels, by inducing an otherwise cryptic promoter located in *pqsD* [195]. When PqsX-T1 or PqsX-T2 were overexpressed,

pqsE transcriptional expression levels rose a hundred times in support of PqsX controlling *pqsE* [195].

The second rotation proposes to elucidate the effect of PqsX on *pqsA*. Firstly, when and to what extend *pqsX* is expressed during PAO1-L growth will be investigated. For this purpose, a PAO1-L *pqsX* reporter strain would be constructed by incorporating the Chilli aptamer [196] near the 3' end of *pqsX*. Chilli is a fluorogen-activating RNA aptamer (FLAP) which mimics large Stokes shift fluorescent proteins when bound to its ligand, DMHBO+ [196]. The advantage of Chllli in comparison to other fluoregen aptamers is the large difference between excitation and emission peaks which offers minimum reabsorption of the emitted light. Once the PqsX-Chilli reporter strain has been constructed, fluorescence levels will be examined and compared to the wild type. If successful, a *pqsA* bioluminescent vector would be transformed to the fluorescent strain with the purpose of measuring expression levels simultaneously. Afterwards, the same experiments would be repeated using other QS deletion mutants, such as *ΔlasR, ΔrhlR* and *ΔpqsR,* to assess how the QS systems regulate *pqsX* expression.

Overall, these findings would suggest an additional layer of regulation of the *pqs* system on the post-transcriptional level. The fact that PqsX appears essential for PYO production, one of the *Pseudomonas* specific virulence factors, and it can circumvent the *pqs* system, could point to a crucial role for PqsX in *P. aeruginosa* virulence. Considering how little is known about *pqsX*, a PhD project could explore a number of different aspects of this sRNA such as: (1) identify gene targets of PqsX, (2) identify protein cofactors of PqsX, (3) phenotypes controlled by PqsX, (4) conditions under which it is expressed, (5) genetic regulation of *pqsX*. Understanding this system regulation and mechanism of action can reveal novel antimicrobial targets, paving the way to the design of antivirulent drugs and adjuvants against *P. aeruginosa.*

Gene targets

Trans-acting sRNAs control gene expression at the post-transcriptional level. PqsX influences the expression of at least one gene at the transcriptional level (*pqsE*) and one at the post-transcriptional level (*pqsA*). It could then be speculated that it regulates post-transcriptionally more genes than *pqsA*, such as other

transcriptional regulators which subsequently alter *pqsE* expression. Wurtzel *et al.* (2012) observed that *pqsX* deletion induced transcription of *prrF1*, *prrF2*, and *antABC* in PA14*.* They reasoned that *antABC* is a target of PqsX thus the increase of anthranilate catabolic enzymes depletes the PYO metabolic pathway from its precursor, the chorismic acid (fig. 15). Furthermore, PqsX induces the expression of *pqsE* and restores PYO synthesis in a *ΔpqsA* mutant, and a *ΔpqsX* mutant does not synthesise PYO. One possible hypothesis could be that PqsX might upregulate the *phz* operons via inducing *pqsE* expression in a *pqsA*-independent way. Deletion of *pqsX* might hinder PqsE induction of PYO synthesis thereby raising anthranilate concentration intracellularly, which would increase *antABC* transcription as a secondary effect. So, it could also be explored whether *antABC* is targeted by PqsX*.* This could be done by constructing bioluminescent or fluorescent reporters for the putative targets and measure their expression levels in absence of or overexpressing PqsX.

The presence of both PqsE and RhlR is prerequisite for activation of the *phz* operons [160]. Furthermore, Rampioni *et al*. (2010) observed that in a PAO1 *ΔpqsE* strain, there is no substantial difference in the *phz* and *lecA* transcript levels when compared to the wild type, despite major differences in production of PYO and Lectin A [150]. It was hypothesised that there could be a post-transcriptional regulatory mechanism or an experimental limitation. If the former was true, then PqsX could mediate post-transcriptional regulation on PYO via PqsE. It would be interesting to assess whether the expression of *pqsX* could circumvent deletion of *pqsE, rhlR,* or both since RhlR is also necessary for PYO production. Collectively, these experiments would indicate a role for PqsX downstream of PqsE and RhlR.

The sRNAs PrrF1 and PrrF2 participate in iron homeostasis of *P. aeuruginosa.* They remain supressed by the iron-dependent regulator Fur in iron-rich conditions [161] (fig. 15). When iron is low, they inhibit translation of *sodB* which is necessary for PYO production in PAO1 [161]. Additionally, they hinder *antR* translation, the transcriptional activator of anthranilate degradation genes *catBCA* and *antABC*, promoting AQ synthesis for iron acquisition [177]. Sakhtah, Price-Whelan, and Dietrich 2013 indicated that, in PAO1 the lack of PrrF sRNAs leads to increased *antR* transcription which contradicts the concurrent upregulation of *antABC* and *prrF1/prrF2* in a PA14 *ΔpqsX* strain [193]. For this reason, it would be

imperative to examine the effect of PqsX on the transcription of *prrF1/prrF2* sRNAs and *antABC* in PAO1 (fig. 15).

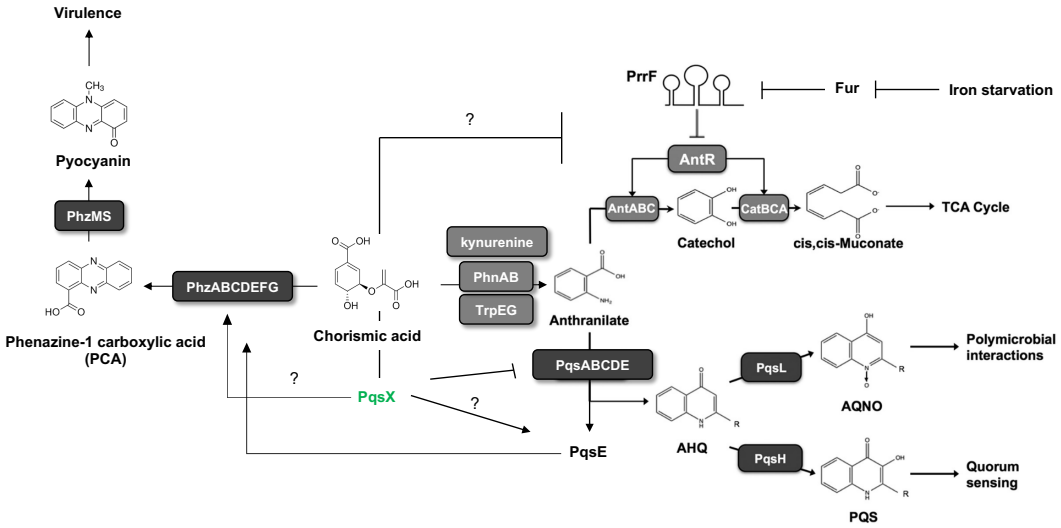

Figure 15. Possible regulatory roles of PqsX in pyocyanin and PQS production. Chorismic acid could follow two avenues: a) it can be metabolised to pyocyanin via the PhzABCDEFG and PhzMS, and b) turned into anthranilate. From there, anthranilate is directed to the production of PQS and other AQ molecules or is catabolised by AntABC and CatBCA enzymes towards the tricarboxylic acid cycle (TCA). Under iron depletion, the ferric uptake regulatory protein (Fur) is suppressed thus unable to inhibit the expression of the Prrf1 and PrrF2 sRNAs. The two PrrF sRNAs can subsequently block the anthranilate regulator AntR expression at the post-transcriptional level, as well as the expression of non-essential iron-containing proteins [197]. As a result, anthranilate is used for PQS production, which acts as an iron trap [114]. In addition, PqsE is produced which promotes PYO production. The sRNA PqsX was shown to downregulate *pqsA* post-transcriptionally, while it could enhance *pqsE* expression and restore PYO synthesis in a *ΔpqsA* mutant [195]. Additionally, it is hypothesised that PqsX inhibits *prrF1/2* and *antAB* expression [193]. However, the mechanism by which PqsX induces PYO production is not known, leading to the possibility of it doing so indirectly, through *pqsE* expression, or directly regulating *phz* operon expression. Adapted from [177].

PqsX induces the expression of *pqsE* from a cryptic promoter upstream of *pqsE* which may be due to the fact that PqsX regulates the expression of a transcriptional regulator of *pqsE* resulting in the effect on this gene. Another explanation could be that PqsX prevents early transcriptional termination of *pqsE* by binding at the 5' UTR and destabilising secondary structures that inhibit transcription. A similar mechanism has been previously described in the

regulation of *rpoS* gene in *E. coli* [198]. This could be demonstrated by creating a transcriptional reporter fusion to the *pqsE* 5' UTR. However, the exact position of *pqsE* cryptic promoter and the TSS are not known. So, another step to be performed first would be to define the TSS of *pqsE.* It could be approached by performing Northern Blot and 5' RACE PCR.

If none of the currently proposed candidates proved to be targets, then a general approach to identify potential target genes could be implemented. Computational tools can predict mRNA targets based on annealing interactions with the sRNA. Some of the currently used programmes are RNApredator [199], intaRNA [200,201], sTarPicker [202], CopraRNA [203], sRNATarget [204], and SPOT [205].

A technique to experimentally find PqsX targets is the GRIL-seq (global small non-coding RNA target identification by ligation and sequencing) [206,207]. Briefly, the sRNA of interest and the bacteriophage T4 RNA ligase are overexpressed under the required experimental conditions. T4 RNA ligase preferentially ligate the monophosphate 5' end to the 3' end of sRNA and mRNA, respectively. Then, the chimeric RNAs can be identified through sequencing. It is a robust technique for the recognition of direct targets of an sRNA in comparison to RNA-seq which could include differentially transcribed RNAs as a secondary effect. The only barrier is the 5′ terminal triphosphate groups in primary transcripts which render the technique dependent on pyrophosphohydrolase RppH for the removal of pyrophosphate from the 5′. Other similar techniques can be found here [208,209].

Subsequently, these genes would be verified both *in vivo* and *in vitro.* Translational fusions of these genes to a reporter would be assessed in the presence or absence of PqsX in PAO1-L. Furthermore, based on the predicted annealed regions of PqsX-target complex, disruptive mutation could be introduced in *pqsX* via site-directed mutagenesis. Then, the impact of these mutations could be measured *in vivo* on translational fusions of the targets*. In vitro* validation could be achieved through Electrophoretic Mobility Shift Assay (EMSA), with or without a putative RNA chaperone, such as Hfq.

Protein cofactors

Another avenue to follow could be detection of cofactors of PqsX. The RNA chaperone Hfq was indicated to directly associate with PqsX and affects *pqsX* transcript levels *in vivo* [193]. Hfq is a Sm-like RNA binding protein present in many bacteria and archae, and a key post-transcriptional regulator [210]. It accelerates and stabilises sRNA-mRNA base-pairing, as well as directly regulates translation of some mRNAs [210]. Interaction of Hfq with a seven poly-U 3' end tail of sRNAs is highly conserved among all bacterial species [210]. Interestingly, PqsX lacks a poly-U stretch at the 3' end (fig. 14C) which makes it less likely to interact with Hfq. Therefore, it would be necessary to validate the binding of PqsX to Hfq performing EMSA. If a direct mRNA target of PqsX was known, then in an *hfq* PAO1 mutant, overexpression of *pqsX* and a translational fusion of the target to a reporter gene could demonstrate the interaction *in vivo.* Any changes to the reporter levels compared to the wild type would indicate PqsX dependence on Hfq.

In the case of no Hfq-PqsX interaction, other methods could be utilised to identify cofactors. One of them could be to crosslink sRNA-protein complexes *in vivo* with UV-irradiation [211]. After RNA isolation, the samples would be probed with biotinylated cDNA specific for the sRNA and the complexes would bind to streptavidin-coated magnetic beads. The final step would be the analysis of attached proteins by liquid chromatography electrospray ionization tandem mass spectrometry (LC-ESI-MS/MS). The most likely hits would be verified via EMSA. Additionally, the regions with which PqsX connects to the protein cofactor could be investigated via RNAse fi footprinting [177,212,213]. Defining the proteins participating in PqsX regulation, coupled with information on its target would provide information on the mechanism of action of PqsX.

Phenotypic characterisation

Since *pqsX* affects PYO production, it would be worth examining what other phenotypes it could affect. Such phenotypes could be elastase and rhamnolipids production, lectin A, biofilm formation, and swarming motility. In all cases, a *pqsX* overexpressing strain, a *ΔpqsX* mutant with and without complementation, and the wild type would be compared. We could also test the impact of PqsX in virulence of QS deletion mutants *ΔlasR, ΔrhlR*, and Δ*pqsR.*

Conditions of expression

The recognition of the conditions under which *pqsX* is expressed could inform on its physiological role. Bacteria deploy sRNAs to quickly adjust in rapid environmental alterations. The change in expression of iron-related sRNAs Prrf1 and Prrf2 could imply a role of PqsX in iron acquisition. Also, the rise in *pqsX* transcription over stationary phase, when oxygen availability is limited, could point to low oxygenation stimulating *pqsX*. Another condition to be tested could be nutrient restriction, such as these in minimal medium because PYO is excreted in response to nutrient starvation [159,214].

Genetic regulation

Apart from QS regulators, *pqsX* expression might be under the influence of other factors. Experimentally, it could be approached by introducing a *pqsX* transcriptional reporter in PAO1 and perform random transposon mutagenesis, either disruptive or inductive.

Another aspect that should be verified is the exact length of the sRNA. The two studies showing the presence of an sRNA in this region do not agree on its size [193,194]. Northern blot and 3' RACE PCR can reveal the exact size of PqsX and the 3' end.

In conclusion, PqsX appears to be a crucial link between the *pqs* system and PYO production, but little is known about the function and direct targets of PqsX. First step in the study of *pqsX* could be to replicate the findings of Wurtzel *et al.* (2012) in PAO1, since PAO1 and PA14 showed differences in the regulation of anthranilate metabolism. Then, it could be explored how PqsX is involved in the regulation of PYO synthesis and under what conditions it is expressed. In parallel, a general search for protein cofactors could be implemented, unless Hfq interaction with PqsX could be shown assisting, in the construction of a mechanistic model of PqsX function. Exploring the influence of PqsX on other virulent factors, for example elastase production could show how broadly the effect of PqsX is on *P. aeruginosa* virulence. An in-depth understanding of the *pqs* system could facilitate the development of sophisticated antivirulence drugs against *P. aeruginosa.* Antivirulence drugs display a few advantages over

traditional antibiotics, such as not promoting AMR at the same levels as antibiotics and that they may cause less harm to the human microbiota [215].

Concluding remarks

The work presented here falls under the umbrella of antimicrobial resistance research and the quest for novel antimicrobial targets. The Gram-negative bacterium *P. aeruginosa* is one of the most threatening MDR pathogens causing high morbidity and mortality rates. Investigating the *pqs* regulatory network of *P. aeruginosa* could potentiate the development of antivirulent drugs, overcoming the selective pressure that current antibiotics impose on this pathogen. Nonetheless, antibiotic penetration of Gram-negative cell wall has slowed down the development of effective antimicrobials. Future antimicrobials and antivirulence drugs, for example a molecule targeting PqsX, would benefit from being able to traverse the cell wall and reach their intracellular targets. A greater understanding of the regulation and events encompassing cell wall division and metabolism, would bring research a step closer to the design of the greatly needed therapeutics. Lastly, analysis of genetic data from outbreaks caused by *Pseudomonas* and other pathogens could shape action plans and aid in recognising patterns of dissemination.

Chapter 5: Bibliography

1. Heynick, F. The original 'magic bullet' is 100 years old. *Br J Psychiatry* **195**, 456–456 (2009).
2. Davies, M. & Walsh, T. R. A colistin crisis in India. *Lancet Infect Dis* **18**, 256–257 (2018).
3. Van, T. T. H., Yidana, Z., Smooker, P. M. & Coloe, P. J. Antibiotic use in food animals worldwide, with a focus on Africa: Pluses and minuses. *J Glob Antimicrob Resist* **20**, 170–177 (2020).
4. WHO. WHO | No Time to Wait: Securing the future from drug-resistant infections. *WHO* http://www.who.int/antimicrobial-resistance/interagency-coordination-group/final-report/en/ (2019).
5. Nicolaou, K. C. & Rigol, S. A brief history of antibiotics and select advances in their synthesis. *J Antibiot* **71**, 153–184 (2018).
6. Fleming, A. On the Antibacterial Action of Cultures of a *Penicillium*, with Special Reference to their Use in the Isolation of B. influenzæ. *Br J Exp Pathol* **10**, 226–236 (1929).
7. Schatz, A. & Waksman, S. A. Effect of Streptomycin and Other Antibiotic Substances upon *Mycobacterium tuberculosis* and Related Organisms.,. *Proc Soc Exp Biol Med* **57**, 244–248 (1944).
8. Eliopoulos, G. M. & Huovinen, P. Resistance to Trimethoprim-Sulfamethoxazole. *Clin Infect Dis* **32**, 1608–1614 (2001).
9. Abraham, E. P. & Chain, E. An enzyme from bacteria able to destroy penicillin. 1940. *Rev. Infect. Dis.* **10**, 677–678 (1988).
10. Jevons, M. P. "Celbenin" - resistant Staphylococci. *Br Med J* **1**, 124–125 (1961).

11. Harkins, C. P. *et al.* Methicillin-resistant *Staphylococcus aureus* emerged long before the introduction of methicillin into clinical practice. *Genome Biol* **18**, (2017).
12. Boneca, I. G. & Chiosis, G. Vancomycin resistance: occurrence, mechanisms and strategies to combat it. *Expert Opin. Ther. Targets* **7**, 311–328 (2003).
13. Levine, D. P. Vancomycin: A History. *Clin Infect Dis* **42**, S5–S12 (2006).
14. Mangili, A., Bica, I., Snydman, D. R. & Hamer, D. H. Daptomycin-Resistant, Methicillin-Resistant *Staphylococcus aureus* Bacteremia. *Clin Infect Dis* **40**, 1058–1060 (2005).
15. Humphries, R. M. *et al.* First Report of Ceftazidime-Avibactam Resistance in a KPC-3-Expressing *Klebsiella pneumoniae* Isolate. *Antimicrob Agents Chemother* **59**, 6605–6607 (2015).
16. Pishchany, G. & Kolter, R. On the possible ecological roles of antimicrobials. *Mol. Biol.* **113**, 580–587 (2020).
17. Romero, D., Traxler, M. F., López, D. & Kolter, R. Antibiotics as Signal Molecules. *Chem Rev* **111**, 5492–5505 (2011).
18. Sengupta, S., Chattopadhyay, M. K. & Grossart, H.-P. The multifaceted roles of antibiotics and antibiotic resistance in nature. *Front Microbiol* **4**, (2013).
19. French, G. L. Bactericidal agents in the treatment of MRSA infections—the potential role of daptomycin. *J Antimicrob Chemother* **58**, 1107–1117 (2006).
20. Aminov, R. History of antimicrobial drug discovery: Major classes and health impact. *Biochem Pharm* **133**, 4–19 (2017).
21. Tenson, T., Lovmar, M. & Ehrenberg, M. The Mechanism of Action of Macrolides, Lincosamides and Streptogramin B Reveals the Nascent Peptide Exit Path in the Ribosome. *J Mol Biol* **330**, 1005–1014 (2003).

22. Coutsogeorgopoulos, C. On the mechanism of action of chloramphenicol in protein synthesis. *Biochim Biophys Acta (BBA) - Nuc Acids Proteins Synth* **129**, 214–217 (1966).

23. Vannuffel, P. & Cocito, C. Mechanism of Action of Streptogramins and Macrolides. *Drugs* **51**, 20–30 (1996).

24. Borghi, A. A., Palma, M. S. A., Borghi, A. A. & Palma, M. S. A. Tetracycline: production, waste treatment and environmental impact assessment. *Braz J Pharm Sci* **50**, 25–40 (2014).

25. Jana, S. & Deb, J. K. Molecular understanding of aminoglycoside action and resistance. *Appl Microbiol Biotechnol* **70**, 140–150 (2006).

26. Patel, U. *et al.* Oxazolidinones Mechanism of Action: Inhibition of the First Peptide Bond Formation. *J. Biol. Chem.* **276**, 37199–37205 (2001).

27. Bozdogan, B. & Appelbaum, P. C. Oxazolidinones: activity, mode of action, and mechanism of resistance. *Int J Antimicrob Agents* **23**, 113–119 (2004).

28. Steenbergen, J. N., Alder, J., Thorne, G. M. & Tally, F. P. Daptomycin: a lipopeptide antibiotic for the treatment of serious Gram-positive infections. *J Antimicrob Chemother* **55**, 283–288 (2005).

29. McClure, W. R. & Cech, C. L. On the mechanism of rifampicin inhibition of RNA synthesis. *J. Biol. Chem.* **253**, 8949–8956 (1978).

30. Bush, K. & Bradford, P. A. β-Lactams and β-Lactamase Inhibitors: An Overview. *Cold Spring Harb Perspect Med* **6**, (2016).

31. Stone, K. J. & Strominger, J. L. Mechanism of Action of Bacitracin: Complexation with Metal Ion and C55-Isoprenyl Pyrophosphate. *PNAS* **68**, 3223–3227 (1971).

32. Binda, E., Marinelli, F. & Marcone, G. L. Old and New Glycopeptide Antibiotics: Action and Resistance. *Antibiotics (Basel)* **3**, 572–594 (2014).

33. Quinlivan, E. P., McPartlin, J., Weir, D. G. & Scott, J. Mechanism of the antimicrobial drug trimethoprim revisited. *The FASEB Journal* **14**, 2519–2524 (2000).

34. Henry, R. J. THE MODE OF ACTION OF SULFONAMIDES *. *Bacteriol Rev* **7**, 175–262 (1943).

35. Lewis, K. Platforms for antibiotic discovery. *Nat Rev Drug Discov* **12**, 371–387 (2013).

36. Morar, M. & Wright, G. D. The Genomic Enzymology of Antibiotic Resistance. *An Rev Genetic* **44**, 25–51 (2010).

37. Finberg, R. W. *et al.* The Importance of Bactericidal Drugs: Future Directions in Infectious Disease. *Clin Infect Dis* **39**, 1314–1320 (2004).

38. D'Costa, V. M. *et al.* Antibiotic resistance is ancient. *Nature* **477**, 457–461 (2011).

39. Davies, J. & Davies, D. Origins and evolution of antibiotic resistance. *Microbiol. Mol. Biol. Rev.* **74**, 417–433 (2010).

40. Wright, G. D. & Poinar, H. Antibiotic resistance is ancient: implications for drug discovery. *Trends Microbiol* **20**, 157–159 (2012).

41. Peterson, E. & Kaur, P. Antibiotic Resistance Mechanisms in Bacteria: Relationships Between Resistance Determinants of Antibiotic Producers, Environmental Bacteria, and Clinical Pathogens. *Front Microbiol* **9**, (2018).

42. Santajit, S. & Indrawattana, N. Mechanisms of Antimicrobial Resistance in ESKAPE Pathogens. *Biomed Res Int* **2016**, (2016).

43. Peirano, G. & Pitout, J. D. D. Extended-Spectrum β-Lactamase-Producing *Enterobacteriaceae*: Update on Molecular Epidemiology and Treatment Options. *Drugs* **79**, 1529–1541 (2019).

44. Baylay, A. J., Piddock, L. J. V. & Webber, M. A. Molecular Mechanisms of Antibiotic Resistance – Part I. in *Bacterial Resistance to Antibiotics – From Molecules to Man* 1–26 (John Wiley & Sons, Ltd, 2019). doi:10.1002/9781119593522.ch1.

45. Peterson, R. M., Huang, T., Rudolf, J. D., Smanski, M. J. & Shen, B. Mechanisms of self-resistance in the platensimycin- and platencin-producing *Streptomyces platensis* MA7327 and MA7339 strains. *Chem. Biol.* **21**, 389–397 (2014).

46. Nikaido, H. & Takatsuka, Y. Mechanisms of RND multidrug efflux pumps. *Biochim. Biophys. Acta* **1794**, 769–781 (2009).

47. Sharkey, L. K. R. & O'Neill, A. J. Molecular Mechanisms of Antibiotic Resistance – Part II. in *Bacterial Resistance to Antibiotics – From Molecules to Man* 27–50 (John Wiley & Sons, Ltd, 2019). doi:10.1002/9781119593522.ch2.

48. von Wintersdorff, C. J. H. *et al.* Dissemination of Antimicrobial Resistance in Microbial Ecosystems through Horizontal Gene Transfer. *Front. Microbiol.* **7**, (2016).

49. The Center for Disease Dynamics, Economics & Policy. ResistanceMap: (2020).

50. ECDC. Surveillance of antimicrobial resistance in Europe 2018. (2018).

51. Gross, M. Antibiotics in crisis. *Curr Biol* **23**, R1063–R1065 (2013).

52. Laxminarayan, R. *et al.* Antibiotic resistance—the need for global solutions. *The Lancet Infectious Diseases* **13**, 1057–1098 (2013).

53. Fleming-Dutra, K. E. *et al.* Prevalence of Inappropriate Antibiotic Prescriptions Among US Ambulatory Care Visits, 2010-2011. *JAMA* **315**, 1864–1873 (2016).

54. Ventola, C. L. The Antibiotic Resistance Crisis. *P T* **40**, 277–283 (2015).

55. Pittet, D. Hand hygiene: From research to action. *J Infect Prev* **18**, 100–102 (2017).

56. Rampling, A. *et al.* Evidence that hospital hygiene is important in the control of methicillin-resistant *Staphylococcus aureus*. *J. Hosp. Infect.* **49**, 109–116 (2001).

57. Frost, I., Van Boeckel, T. P., Pires, J., Craig, J. & Laxminarayan, R. Global geographic trends in antimicrobial resistance: the role of international travel. *J Travel Med* **26**, (2019).

58. Bengtsson-Palme, J. *et al.* The Human Gut Microbiome as a Transporter of Antibiotic Resistance Genes between Continents. *Antimicrob Agents Chemother* **59**, 6551–6560 (2015).

59. Towse, A. *et al.* Time for a change in how new antibiotics are reimbursed: Development of an insurance framework for funding new antibiotics based on a policy of risk mitigation. *Health Policy* **121**, 1025–1030 (2017).

60. Payne, D. J., Gwynn, M. N., Holmes, D. J. & Pompliano, D. L. Drugs for bad bugs: confronting the challenges of antibacterial discovery. *Nat Rev Drug Discov***6**, 29–40 (2007).

61. Mullard, A. Achaogen bankruptcy highlights antibacterial development woes. *Nat Rev Drug Discov* **18**, 411–412 (2019).

62. Desnoyers, G., Bouchard, M.-P. & Massé, E. New insights into small RNA-dependent translational regulation in prokaryotes. *Trends Genetic* **29**, 92–98 (2013).

63. EvaluatePharma. World Preview 2019, Outlook to 2024. (2019).

64. Årdal, C. *et al.* Antibiotic development — economic, regulatory and societal challenges. *Nature Reviews Microbiology* **18**, 267–274 (2020).

65. Dadgostar, P. Antimicrobial Resistance: Implications and Costs. *Infect Drug Resist* **12**, 3903–3910 (2019).

66. Shrestha, P. *et al.* Enumerating the economic cost of antimicrobial resistance per antibiotic consumed to inform the evaluation of interventions affecting their use. *Antimicrob Resist Infect Control* **7**, 98 (2018).

67. CDC. *Antibiotic resistance threats in the United States, 2019*. https://stacks.cdc.gov/view/cdc/82532 (2019) doi:10.15620/cdc:82532.

68. Jonas, O. B., Irwin, A., Berthe, F. C. J., Le Gall, F. G. & Marquez, P. V. *Drug-resistant infections : a threat to our economic future (Vol. 2) : final report (English)*.1–172 http://documents.worldbank.org/curated/en/323311493396993758/final-report (2017).

69. George, A. Antimicrobial Resistance (AMR) in the Food Chain: Trade, One Health and Codex. *Trop Med Infect Dis* **4**, (2019).

70. CDC. Antibiotic-resistant Germs: New Threats. *Centers for Disease Control and Prevention* https://www.cdc.gov/drugresistance/biggest-threats.html (2020).

71. WHO. Prioritization of pathogens to guide discovery, research and development of new antibiotics for drug resistant bacterial infections, including tuberculosis. *WHO*
http://www.who.int/medicines/areas/rational_use/prioritization-of-pathogens/en/ (2017).
72. O'Neill, J. Antimicrobial resistance: tackling a crisis for the health and wealth of nations. (2014).
73. Roemer, T. & Krysan, D. J. Antifungal Drug Development: Challenges, Unmet Clinical Needs, and New Approaches. *Cold Spring Harb Perspect Med* **4**, a019703 (2014).
74. Prasad, R., Shah, A. H. & Rawal, M. K. Antifungals: Mechanism of Action and Drug Resistance. in *Yeast Membrane Transport* (eds. Ramos, J., Sychrová, H. & Kschischo, M.) 327–349 (Springer International Publishing, 2016). doi:10.1007/978-3-319-25304-6_14.
75. Lai, C.-C., Tan, C.-K., Huang, Y.-T., Shao, P.-L. & Hsueh, P.-R. Current challenges in the management of invasive fungal infections. *J. Infect. Chemother.* **14**, 77–85 (2008).
76. Butts, A. & Krysan, D. J. Antifungal Drug Discovery: Something Old and Something New. *PLoS Pathog* **8**, (2012).
77. Park, B. J. *et al.* Estimation of the current global burden of cryptococcal meningitis among persons living with HIV/AIDS. *AIDS* **23**, 525–530 (2009).
78. Uchil, R. R., Kohli, G. S., Katekhaye, V. M. & Swami, O. C. Strategies to Combat Antimicrobial Resistance. *J Clin Diagn Res* **8**, ME01–ME04 (2014).

79. Duerden, B., Fry, C., Johnson, A. P. & Wilcox, M. H. The Control of Methicillin-Resistant *Staphylococcus aureus* Blood Stream Infections in England. *Open Forum Infect Dis* **2**, (2015).

80. O'Neill, J. Tackling Drug-Resistant Infections Globally: Final Report And Recommendations. (2016).

81. Årdal, C. *et al.* Revitalizing the antibiotic pipeline. (2018).

82. McCarthy, M. W. Clinical Pharmacokinetics and Pharmacodynamics of Eravacycline. *Clin Pharmacokinet* **58**, 1149–1153 (2019).

83. Imai, Y. *et al.* A new antibiotic selectively kills Gram-negative pathogens. *Nature* **576**, 459–464 (2019).

84. Codjoe, F. S. & Donkor, E. S. Carbapenem Resistance: A Review. *Med Sci (Basel)* **6**, (2017).

85. Lebreton, F. & Cattoir, V. Resistance to Glycopeptide Antibiotics. in *Bacterial Resistance to Antibiotics – From Molecules to Man* 51–80 (John Wiley & Sons, Ltd, 2019). doi:10.1002/9781119593522.ch3.

86. Goodwin, S., McPherson, J. D. & McCombie, W. R. Coming of age: ten years of next-generation sequencing technologies. *Nat Rev Genet* **17**, 333–351 (2016).

87. Otto, M. Next-generation sequencing to monitor the spread of antimicrobial resistance. *Gen Med* **9**, 68 (2017).

88. Kline, T., B. Felise, H., Sanowar, S. & I. Miller, S. The Type III Secretion System as a Source of Novel Antibacterial Drug Targets. *Curr Drug Tar* **13**, 338–351 (2012).

89. Steadman, D., Lo, A., Waksman, G. & Remaut, H. Bacterial surface appendages as targets for novel antibacterial therapeutics. *Fut Microbiol* **9**, 887–900 (2014).

90. Escaich, S. Novel agents to inhibit microbial virulence and pathogenicity. *Expert Opin Ther Pat* **20**, 1401–1418 (2010).

91. Mühlen, S. & Dersch, P. Anti-virulence Strategies to Target Bacterial Infections. in *How to Overcome the Antibiotic Crisis : Facts, Challenges, Technologies and Future Perspectives* (eds. Stadler, M. & Dersch, P.) 147–183 (Springer International Publishing, 2016). doi:10.1007/82_2015_490.

92. Williams, P. & Cámara, M. Quorum sensing and environmental adaptation in *Pseudomonas aeruginosa*: a tale of regulatory networks and multifunctional signal molecules. *Curr Opin Microbiol* **12**, 182–191 (2009).

93. Heeb, S. *et al.* Quinolones: from antibiotics to autoinducers. *FEMS Microbiol Rev* **35**, 247–274 (2011).

94. Baldelli, V. *et al.* Identification of FDA-approved antivirulence drugs targeting the *Pseudomonas aeruginosa* quorum sensing effector protein PqsE. *Virulence* **0**, null (2020).

95. Soukarieh, F., Williams, P., Stocks, M. J. & Cámara, M. *Pseudomonas aeruginosa* Quorum Sensing Systems as Drug Discovery Targets: Current Position and Future Perspectives. *J. Med. Chem.* **61**, 10385–10402 (2018).

96. Silhavy, T. J., Kahne, D. & Walker, S. The Bacterial Cell Envelope. *Cold Spring Harb Perspect Biol* **2**, (2010).

97. Typas, A., Banzhaf, M., Gross, C. A. & Vollmer, W. From the regulation of peptidoglycan synthesis to bacterial growth and morphology. *Nat. Rev. Microbiol.* **10**, 123–136 (2011).

98. Uehara, T., Parzych, K. R., Dinh, T. & Bernhardt, T. G. Daughter cell separation is controlled by cytokinetic ring-activated cell wall hydrolysis. *EMBO J* **29**, 1412–1422 (2010).

99. Du, S. & Lutkenhaus, J. Assembly and Activation of the *Escherichia coli* Divisome. *Mol Microbiol* **105**, 177–187 (2017).

100. Weiss, D. S. Bacterial cell division and the septal ring. *Mol. Microbiol.* **54**, 588–597 (2004).

101. Egan, A. J. F., Errington, J. & Vollmer, W. Regulation of peptidoglycan synthesis and remodelling. *Na Rev Microbiol* **18**, 446–460 (2020).

102. Lupoli, T. J. *et al.* Studying a cell division amidase using defined peptidoglycan substrates. *J. Am. Chem. Soc.* **131**, 18230–18231 (2009).

103. Peters, N. T., Dinh, T. & Bernhardt, T. G. A Fail-Safe Mechanism in the Septal Ring Assembly Pathway Generated by the Sequential Recruitment of Cell Separation Amidases and Their Activators ▿. *J Bacteriol* **193**, 4973–4983 (2011).

104. Heidrich, C. *et al.* Involvement of N-acetylmuramyl-L-alanine amidases in cell separation and antibiotic-induced autolysis of *Escherichia coli*. *Mol. Microbiol.* **41**, 167–178 (2001).

105. Tsang, M.-J., Yakhnina, A. A. & Bernhardt, T. G. NlpD links cell wall remodelling and outer membrane invagination during cytokinesis in *Escherichia coli*. *PLOS Genetics* **13**, e1006888 (2017).

106. Singh, S. K., Parveen, S., SaiSree, L. & Reddy, M. Regulated proteolysis of a cross-link-specific peptidoglycan hydrolase contributes to bacterial morphogenesis. *Proc. Natl. Acad. Sci. U.S.A.* **112**, 10956–10961 (2015).

107. Banzhaf, M. *et al.* Outer membrane lipoprotein NlpI scaffolds peptidoglycan hydrolases within multi-enzyme complexes in *Escherichia coli*. *The EMBO Journal* **39**, e102246 (2020).

108. Wilson, C. G. M., Kajander, T. & Regan, L. The crystal structure of NlpI. A prokaryotic tetratricopeptide repeat protein with a globular fold. *FEBS J.* **272**, 166–179 (2005).

109. Zeytuni, N. & Zarivach, R. Structural and Functional Discussion of the Tetra-Trico-Peptide Repeat, a Protein Interaction Module. *Structure* **20**, 397–405 (2012).

110. Jerabek-Willemsen, M. *et al.* MicroScale Thermophoresis: Interaction analysis and beyond. *J Mol Struct* **1077**, 101–113 (2014).

111. Lynch, T., Petkau, A., Knox, N., Graham, M. & Domselaar, G. V. A Primer on Infectious Disease Bacterial Genomics. *Clin Microbiol Rev* **29**, 881–913 (2016).

112. Petitjean, M. *et al.* Genomic characterization of a local epidemic *Pseudomonas aeruginosa* reveals specific features of the widespread clone ST395. *Microb Genom* **3**, (2017).

113. Bhagirath, A. Y. *et al.* Cystic fibrosis lung environment and *Pseudomonas aeruginosa* infection. *BMC Pulm Med* **16**, (2016).

114. Lin, J., Cheng, J., Wang, Y. & Shen, X. The *Pseudomonas Quinolone* Signal (PQS): Not Just for Quorum Sensing Anymore. *Front. Cell. Infect. Microbiol.* **8**, (2018).

115. Oliver, A., Mulet, X., López-Causapé, C. & Juan, C. The increasing threat of *Pseudomonas aeruginosa* high-risk clones. *Drug Resist. Updat.* **21–22**, 41–59 (2015).

116. Bertrand, X. *et al.* Large outbreak in a surgical intensive care unit of colonization or infection with *Pseudomonas aeruginosa* that overexpressed an active efflux pump. *Clin. Infect. Dis.* **31**, E9–E14 (2000).

117. Quick, J. *et al.* Seeking the source of *Pseudomonas aeruginosa* infections in a recently opened hospital: an observational study using whole-genome sequencing. *BMJ Open* **4**, e006278 (2014).

118. Kipnis, E., Sawa, T. & Wiener-Kronish, J. Targeting mechanisms of *Pseudomonas aeruginosa* pathogenesis. *Médecine et Maladies Infectieuses* **36**, 78–91 (2006).

119. Valot, B. *et al.* What It Takes to Be a Pseudomonas aeruginosa? The Core Genome of the Opportunistic Pathogen Updated. *PLOS ONE* **10**, e0126468 (2015).

120. Ozer, E. A., Allen, J. P. & Hauser, A. R. Characterization of the core and accessory genomes of *Pseudomonas aeruginosa* using bioinformatic tools Spine and AGEnt | BMC Genomics | Full Text. *BMC Genomics* (2014).

121. Kung, V. L., Ozer, E. A. & Hauser, A. R. The Accessory Genome of *Pseudomonas aeruginosa*. *Microbiol. Mol. Biol. Rev.* **74**, 621–641 (2010).

122. Martin, M. Cutadapt removes adapter sequences from high-throughput sequencing reads. *EMBnet.journal* **17**, 10–12 (2011).

123. Gurevich, A., Saveliev, V., Vyahhi, N. & Tesler, G. QUAST: quality assessment tool for genome assemblies. *Bioinformatics* **29**, 1072–1075 (2013).

124. Seemann, T. Prokka: rapid prokaryotic genome annotation. *Bioinformatics* **30**, 2068–2069 (2014).

125. Jolley, K. A. & Maiden, M. C. BIGSdb: Scalable analysis of bacterial genome variation at the population level. *BMC Bioinformatics* **11**, 595 (2010).

126. Page, A. J. *et al.* Roary: rapid large-scale prokaryote pan genome analysis. *Bioinformatics* **31**, 3691–3693 (2015).

127. Seemann, T. *tseemann/snippy*. (2020).

128. Stamatakis, A. RAxML-VI-HPC: maximum likelihood-based phylogenetic analyses with thousands of taxa and mixed models. *Bioinformatics* **22**, 2688–2690 (2006).

129. Treangen, T. J., Ondov, B. D., Koren, S. & Phillippy, A. M. The Harvest suite for rapid core-genome alignment and visualization of thousands of intraspecific microbial genomes. *Genome Biol* **15**, (2014).

130. Hadfield, J. *et al.* Phandango: an interactive viewer for bacterial population genomics. *Bioinformatics* **34**, 292–293 (2018).

131. Feldgarden, M. *et al.* Validating the AMRFinder Tool and Resistance Gene Database by Using Antimicrobial Resistance Genotype-Phenotype Correlations in a Collection of Isolates. *Antimicrob Agents Chemother* **63**, (2019).

132. McInerney, J. O., McNally, A. & O'Connell, M. J. Why prokaryotes have pangenomes. *Na Microbiol* **2**, 1–5 (2017).

133. Rehm, B. H. A. *Pseudomonas: Model Organism, Pathogen, Cell Factory*. (John Wiley & Sons, 2008).

134. Marçais, G. *et al.* MUMmer4: A fast and versatile genome alignment system. *PLoS Comput. Biol.* **14**, e1005944 (2018).

135. Guindon, S. *et al.* New algorithms and methods to estimate maximum-likelihood phylogenies: assessing the performance of PhyML 3.0. *Syst. Biol.* **59**, 307–321 (2010).

136. Jeukens, J. *et al.* Comparative genomics of isolates of a *Pseudomonas aeruginosa* epidemic strain associated with chronic lung infections of cystic fibrosis patients. *PLoS ONE* **9**, e87611 (2014).

137. Valot, B. *et al.* Comparative Genomic Analysis of Two Multidrug-Resistant Clinical Isolates of ST395 Epidemic Strain of *Pseudomonas aeruginosa* Obtained 12 Years Apart. *Genome Announc.* **2**, (2014).

138. Morales-Espinosa, R. *et al.* Fingerprint Analysis and Identification of Strains ST309 as a Potential High Risk Clone in a *Pseudomonas aeruginosa* Population Isolated from Children with Bacteremia in Mexico City. *Front. Microbiol.* **8**, (2017).

139. Koutsogiannou, M. *et al.* Spread of Multidrug-Resistant *Pseudomonas aeruginosa* Clones in a University Hospital. *J Clin Microbiol* **51**, 665–668 (2013).

140. Khan, A. *et al.* Extensively Drug-Resistant Pseudomonas aeruginosa ST309 Harboring Tandem Guiana Extended Spectrum β-Lactamase Enzymes: A Newly Emerging Threat in the United States. *Open Forum Infect Dis* **6**, ofz273 (2019).

141. Deredjian, A. *et al.* Antibiotic and metal resistance among hospital and outdoor strains of *Pseudomonas aeruginosa*. *Res Microbiol* **162**, 689–700 (2011).

142. Souli, M. *et al.* Antimicrobial activity of copper surfaces against carbapenemase-producing contemporary Gram-negative clinical isolates. *J Antimicrob Chemother* **68**, 852–857 (2013).

143. WHO, E. Global Priority List Of Antibiotic-Resistant Bacteria To Guide Research, Discovery, And Development Of New Antibiotics. 7 (2017).

144. Darch, S. E. *et al.* Spatial determinants of quorum signaling in a *Pseudomonas aeruginosa* infection model. *PNAS* **115**, 4779–4784 (2018).

145. Kang, D. *et al.* Pyoverdine-Dependent Virulence of *Pseudomonas aeruginosa* Isolates From Cystic Fibrosis Patients. *Front. Microbiol.* **10**, (2019).

146. Pang, Z., Raudonis, R., Glick, B. R., Lin, T.-J. & Cheng, Z. Antibiotic resistance in *Pseudomonas aeruginosa*: mechanisms and alternative therapeutic strategies. *Biotechnol Adv* **37**, 177–192 (2019).

147. Dubern, J.-F. *et al.* Integrated whole-genome screening for *Pseudomonas aeruginosa* virulence genes using multiple disease models reveals that pathogenicity is host specific. *Environ Microbiol* **17**, 4379–4393 (2015).

148. Hentzer, M. & Givskov, M. Pharmacological inhibition of quorum sensing for the treatment of chronic bacterial infections. *J Clin Invest* **112**, 1300–1307 (2003).

149. Rampioni, G. *et al.* Unravelling the Genome-Wide Contributions of Specific 2-Alkyl-4-Quinolones and PqsE to Quorum Sensing in *Pseudomonas aeruginosa. PLOS Pathogens* **12**, e1006029 (2016).

150. Rampioni, G. *et al.* Transcriptomic analysis reveals a global alkyl-quinolone-independent regulatory role for PqsE in facilitating the environmental adaptation of *Pseudomonas aeruginosa* to plant and animal hosts. *Environ Microbiol* **12**, 1659–1673 (2010).

151. Lépine, F., Milot, S., Déziel, E., He, J. & Rahme, L. G. Electrospray/mass spectrometric identification and analysis of 4-hydroxy-2-alkylquinolines (HAQs) produced by *Pseudomonas aeruginosa*. *J Am Soc Mass Spectrom* **15**, 862–869 (2004).

152. Farrow, J. M. & Pesci, E. C. Two distinct pathways supply anthranilate as a precursor of the *Pseudomonas* quinolone signal. *J. Bacteriol.* **189**, 3425–3433 (2007).

153. Knoten, C. A., Wells, G., Coleman, J. P. & Pesci, E. C. A Conserved Suppressor Mutation in a Tryptophan Auxotroph Results in Dysregulation of *Pseudomonas Quinolone* Signal Synthesis. *J. Bacteriol.* **196**, 2413–2422 (2014).

154. Zhang, Y.-M., Frank, M. W., Zhu, K., Mayasundari, A. & Rock, C. O. PqsD Is Responsible for the Synthesis of 2,4-Dihydroxyquinoline, an Extracellular Metabolite Produced by *Pseudomonas aeruginosa*. *J. Biol. Chem.* **283**, 28788–28794 (2008).

155. Coleman, J. P. *et al.* Pseudomonas aeruginosa PqsA Is an Anthranilate-Coenzyme A Ligase. *J. Bacteriol.* **190**, 1247–1255 (2008).

156. Drees, S. L. *et al.* PqsBC, a Condensing Enzyme in the Biosynthesis of the *Pseudomonas aeruginosa* Quinolone Signal Crystal Structure, Inhibition, and Reaction Mechanism. *J. Biol. Chem.* **291**, 6610–6624 (2016).

157. Drees, S. L. & Fetzner, S. PqsE of Pseudomonas aeruginosa Acts as Pathway-Specific Thioesterase in the Biosynthesis of Alkylquinolone Signaling Molecules. *Chemistry & Biology* **22**, 611–618 (2015).

158. Schertzer, J. W., Brown, S. A. & Whiteley, M. Oxygen levels rapidly modulate *Pseudomonas aeruginosa* social behaviours via substrate limitation of PqsH. *Mol. Biol.* **77**, 1527–1538 (2010).

159. Price-Whelan, A., Dietrich, L. E. P. & Newman, D. K. Rethinking 'secondary' metabolism: physiological roles for phenazine antibiotics. *Nat Chem Biol* **2**, 71–78 (2006).

160. Higgins, S. *et al.* Differential Regulation of the Phenazine Biosynthetic Operons by Quorum Sensing in *Pseudomonas aeruginosa* PAO1-N. *Front Cell Infect Microbiol* **8**, (2018).

161. Sakhtah, H., Price-Whelan, A. & Dietrich, L. E. P. Regulation of Phenazine Biosynthesis. in *Microbial Phenazines: Biosynthesis, Agriculture and Health* (eds. Chincholkar, S. & Thomashow, L.) 19–42 (Springer, 2013). doi:10.1007/978-3-642-40573-0_2.

162. McKnight, S. L., Iglewski, B. H. & Pesci, E. C. The *Pseudomonas* Quinolone Signal Regulates rhl Quorum Sensing in *Pseudomonas aeruginosa*. *J Bacteriol* **182**, 2702–2708 (2000).

163. Cao, H. *et al.* A quorum sensing-associated virulence gene of *Pseudomonas aeruginosa* encodes a LysR-like transcription regulator with a unique self-regulatory mechanism. *Proc. Natl. Acad. Sci. U.S.A.* **98**, 14613–14618 (2001).

164. McGrath, S., Wade, D. S. & Pesci, E. C. Dueling quorum sensing systems in *Pseudomonas aeruginosa* control the production of the *Pseudomonas quinolone signal* (PQS). *FEMS Microbiol. Lett.* **230**, 27–34 (2004).

165. Gallagher, L. A., McKnight, S. L., Kuznetsova, M. S., Pesci, E. C. & Manoil, C. Functions Required for Extracellular Quinolone Signaling by *Pseudomonas aeruginosa*. *J. Bacteriol.* **184**, 6472–6480 (2002).

166. Xiao, G. *et al.* MvfR, a key *Pseudomonas aeruginosa* pathogenicity LTTR-class regulatory protein, has dual ligands. *Mol. Microbiol.* **62**, 1689–1699 (2006).

167. Kang, H. *et al.* Crystal structure of *Pseudomonas aeruginosa* RsaL bound to promoter DNA reaffirms its role as a global regulator involved in quorum-sensing. *Nucleic Acids Res* **45**, 699–710 (2017).

168. Sonnleitner, E. *et al.* The small RNA PhrS stimulates synthesis of the Pseudomonas aeruginosa quinolone signal. *Mol. Biol.* **80**, 868–885 (2011).

169. Farrow, J. M. & Pesci, E. C. Distal and proximal promoters co-regulate *pqsR* expression in *Pseudomonas aeruginosa*. *Mol Microbiol* **104**, 78–91 (2017).

170. Liang, H., Li, L., Dong, Z., Surette, M. G. & Duan, K. The YebC Family Protein PA0964 Negatively Regulates the *Pseudomonas aeruginosa* Quinolone Signal System and Pyocyanin Production. *J. Bacteriol.* **190**, 6217–6227 (2008).

171. Hazan, R. *et al.* Homeostatic Interplay between Bacterial Cell-Cell Signaling and Iron in Virulence. *PLoS Pathog* **6**, (2010).

172. Wade, D. S. *et al.* Regulation of Pseudomonas Quinolone Signal Synthesis in Pseudomonas aeruginosa. *J. Bacteriol.* **187**, 4372–4380 (2005).

173. Diggle, S. P. *et al.* The *Pseudomonas aeruginosa* quinolone signal molecule overcomes the cell density-dependency of the quorum sensing hierarchy, regulates rhl-dependent genes at the onset of stationary phase and can be produced in the absence of LasR. *Mol. Microbiol.* **50**, 29–43 (2003).

174. Xiao, G., He, J. & Rahme, L. G. Mutation analysis of the *Pseudomonas aeruginosa mvfR* and *pqsABCDE* gene promoters demonstrates complex quorum-sensing circuitry. *Microbiol.,* **152**, 1679–1686 (2006).

175. Brouwer, S. *et al.* The PqsR and RhlR Transcriptional Regulators Determine the Level of Pseudomonas Quinolone Signal Synthesis in *Pseudomonas aeruginosa* by Producing Two Different *pqsABCDE* mRNA Isoforms. *J. Bacteriol.* **196**, 4163–4171 (2014).

176. Carloni, S., Macchi, R., Sattin, S., Ferrara, S. & Bertoni, G. The small RNA ReaL: a novel regulatory element embedded in the *Pseudomonas aeruginosa* quorum sensing networks. *Environ. Microbio.* **19**, 4220–4237 (2017).

177. Djapgne, L. *et al.* The *Pseudomonas aeruginosa* PrrF1 and PrrF2 Small Regulatory RNAs Promote 2-Alkyl-4-Quinolone Production through Redundant Regulation of the antR mRNA. *J. Bacteriol.y* **200**, (2018).

178. Tahrioui, A. *et al.* Extracellular DNA release, quorum sensing, and PrrF1/F2 small RNAs are key players in *Pseudomonas aeruginosa* tobramycin-enhanced biofilm formation. *npj Biofilms Microbiomes* **5**, 1–11 (2019).

179. Thomason, M. K. *et al.* A rhlI 5′ UTR-Derived sRNA Regulates RhlR-Dependent Quorum Sensing in *Pseudomonas aeruginosa*. *mBio* **10**, (2019).

180. Malgaonkar, A. & Nair, M. Quorum sensing in *Pseudomonas aeruginosa* mediated by RhlR is regulated by a small RNA PhrD. *Sci Rep* **9**, 1–11 (2019).

181. Huang, J., Sonnleitner, E., Ren, B., Xu, Y. & Haas, D. Catabolite Repression Control of Pyocyanin Biosynthesis at an Intersection of Primary and Secondary Metabolism in *Pseudomonas aeruginosa*. *Appl. Environ. Microbiol.* **78**, 5016–5020 (2012).

182. Goodman, A. L. *et al.* Direct interaction between sensor kinase proteins mediates acute and chronic disease phenotypes in a bacterial pathogen. *Genes Dev.* **23**, 249–259 (2009).

183. Janssen, K. H., Diaz, M. R., Gode, C. J., Wolfgang, M. C. & Yahr, T. L. RsmV, a Small Noncoding Regulatory RNA in *Pseudomonas aeruginosa* That Sequesters RsmA and RsmF from Target mRNAs. *J. Bacteriol.* **200**, (2018).

184. Romero, M. *et al.* Genome-wide mapping of the RNA targets of the *Pseudomonas aeruginosa* riboregulatory protein RsmN. *Nucleic Acids Res* **46**, 6823–6840 (2018).

185. Wagner, E. G. H. & Romby, P. Chapter Three - Small RNAs in Bacteria and Archaea: Who They Are, What They Do, and How They Do It. in *Advances in Genetics* (eds. Friedmann, T., Dunlap, J. C. & Goodwin, S. F.) vol. 90 133–208 (Academic Press, 2015).

186. Chen, J., Morita, T. & Gottesman, S. Regulation of Transcription Termination of Small RNAs and by Small RNAs: Molecular Mechanisms and Biological Functions. *Front. Cell. Infect. Microbiol.* (2019) doi:10.3389/fcimb.2019.00201.

187. Gottesman, S. & Storz, G. Bacterial Small RNA Regulators: Versatile Roles and Rapidly Evolving Variations. *Cold Spring Harb Perspect Biol* **3**, a003798 (2011).

188. Papenfort, K. & Vanderpool, C. K. Target activation by regulatory RNAs in bacteria. *FEMS Microbiol Rev* **39**, 362–378 (2015).

189. Dutta, T. & Srivastava, S. Small RNA-mediated regulation in bacteria: A growing palette of diverse mechanisms. *Gene* **656**, 60–72 (2018).

190. Smirnov, A., Wang, C., Drewry, L. L. & Vogel, J. Molecular mechanism of mRNA repression *in trans* by a ProQ-dependent small RNA. *The EMBO Journal* **36**, 1029–1045 (2017).

191. Olejniczak, M. & Storz, G. ProQ/FinO-domain proteins: another ubiquitous family of RNA matchmakers? *Mol.r Microbiol.* **104**, 905–915 (2017).

192. Dötsch, A. *et al.* The *Pseudomonas aeruginosa* Transcriptome in Planktonic Cultures and Static Biofilms Using RNA Sequencing. *PLOS ONE* **7**, e31092 (2012).

193. Wurtzel, O. *et al.* The Single-Nucleotide Resolution Transcriptome of *Pseudomonas aeruginosa* Grown in Body Temperature. *PLOS Pathog.* **8**, e1002945 (2012).

194. Gómez-Lozano, M., Marvig, R. L., Molin, S. & Long, K. S. Genome-wide identification of novel small RNAs in *Pseudomonas aeruginosa*. *Environ. Microbiol* **14**, 2006–2016 (2012).

195. Romo Catalan, N. Regulation of the PQS Quorum sensing operon in *Pseudomonas aeruginosa* by the effector PqsE. (unpublished data). (2020).

196. Steinmetzger, C., Palanisamy, N., Gore, K. R. & Höbartner, C. A Multicolor Large Stokes Shift Fluorogen-Activating RNA Aptamer with Cationic Chromophores. *Chemistry* **25**, 1931–1935 (2019).

197. Wilderman, P. J. *et al.* Identification of tandem duplicate regulatory small RNAs in *Pseudomonas aeruginosa* involved in iron homeostasis. *Proc Natl Acad Sci U S A* **101**, 9792–9797 (2004).

198. Sedlyarova, N. *et al.* sRNA-Mediated Control of Transcription Termination in E. coli. *Cell* **167**, 111-121.e13 (2016).

199. Eggenhofer, F., Tafer, H., Stadler, P. F. & Hofacker, I. L. RNApredator: fast accessibility-based prediction of sRNA targets. *Nucleic Acids Res* **39**, W149–W154 (2011).

200. Busch, A., Richter, A. S. & Backofen, R. IntaRNA: efficient prediction of bacterial sRNA targets incorporating target site accessibility and seed regions. *Bioinformatics* **24**, 2849–2856 (2008).

201. Mann, M., Wright, P. R. & Backofen, R. IntaRNA 2.0: enhanced and customizable prediction of RNA-RNA interactions. *Nucleic Acids Res.* **45**, W435–W439 (2017).

202. Ying, X. *et al.* sTarPicker: a method for efficient prediction of bacterial sRNA targets based on a two-step model for hybridization. *PLoS ONE* **6**, e22705 (2011).

203. Wright, P. R. *et al.* Comparative genomics boosts target prediction for bacterial small RNAs. *Proc. Natl. Acad. Sci. U.S.A.* **110**, E3487-3496 (2013).

204. Cao, Y. *et al.* sRNATarget: a web server for prediction of bacterial sRNA targets. *Bioinformation* **3**, 364–366 (2009).

205. King, A. M., Vanderpool, C. K. & Degnan, P. H. sRNA Target Prediction Organizing Tool (SPOT) Integrates Computational and Experimental Data To Facilitate Functional Characterization of Bacterial Small RNAs. *mSphere* **4**, (2019).

206. Han, K., Tjaden, B. & Lory, S. GRIL-seq provides a method for identifying direct targets of bacterial small regulatory RNA by in vivo proximity ligation. *Nat Microbiol* **2**, 1–10 (2016).

207. Zhang, Y.-F. *et al.* Probing the sRNA regulatory landscape of *P. aeruginosa*: post-transcriptional control of determinants of pathogenicity and antibiotic susceptibility. *Mol. Microbiol.* **106**, 919–937 (2017).

208. Lalaouna, D. & Massé, E. Identification of sRNA interacting with a transcript of interest using MS2-affinity purification coupled with RNA sequencing (MAPS) technology. *Genom Data* **5**, 136–138 (2015).

209. Melamed, S. *et al.* Global Mapping of Small RNA-Target Interactions in Bacteria. *Mol. Cell* **63**, 884–897 (2016).

210. Santiago-Frangos, A. & Woodson, S. A. Hfq chaperone brings speed dating to bacterial sRNA. *WIREs RNA* **9**, e1475 (2018).

211. Osborne, J., Djapgne, L., Tran, B. Q., Goo, Y. A. & Oglesby-Sherrouse, A. G. A method for *in vivo* identification of bacterial small RNA-binding proteins. *MicrobiologyOpen* **3**, 950–960 (2014).

212. Nilsen, T. W. RNase Footprinting to Map Sites of RNA–Protein Interactions. *Cold Spring Harb Protoc* **2014**, pdb.prot080788 (2014).

213. Yi, P., Soper, T. J. & Woodson, S. A. RNase footprinting of protein binding sites on an mRNA target of small RNAs. *Methods Mol Biol* **905**, 213–224 (2012).

214. Wang, R., Starkey, M., Hazan, R. & Rahme, L. G. Honey's Ability to Counter Bacterial Infections Arises from Both Bactericidal Compounds and QS Inhibition. *Front Microbiol* **3**, (2012).

215. Dickey, S. W., Cheung, G. Y. C. & Otto, M. Different drugs for bad bugs: antivirulence strategies in the age of antibiotic resistance. *Nature Reviews Drug Discovery* **16**, 457–471 (2017).